Mechatronics xxx (2012) xxx–xxx

Contents lists available at SciVerse ScienceDirect

Mechatronics

journal homepage: www.elsevier.com/locate/mechatronics

Design and construction of a novel quad tilt-wing UAV

E. Cetinsoy, S. Dikyar, C. Hancer, K.T. Oner, E. Sirimoglu, M. Unel *, M.F. Aksit

Faculty of Engineering and Natural Sciences, Sabanci University, Orhanli-Tuzla, Istanbul, Turkey

ARTICLE INFO

Article history:
Received 26 November 2010
Accepted 12 March 2012
Available online xxxx

Keywords:
UAV
Quad tilt-wing
Aerodynamic design
Carbon composite
Hierarchical control system

ABSTRACT

This paper presents aerodynamic and mechanical design, prototyping and flight control system design of a new unmanned aerial vehicle SUAVI (Sabanci University Unmanned Aerial VehIcle). SUAVI is an electric powered quad tilt-wing UAV that is capable of vertical takeoff and landing (VTOL) like a helicopter and long duration horizontal flight like an airplane. Aerodynamic and mechanical designs are optimized to enhance the operational performance of the aerial vehicle. Both of them have great importance for increasing efficiency, reaching the flight duration goals and achieving the desired tasks. A full dynamical model is derived by utilizing Newton–Euler formulation for the development of the flight control system. The prototype is constructed from carbon composite material. A hierarchical control system is designed where a high level controller (supervisor) is responsible for task decision, monitoring states of the vehicle, generating references for low level controllers, etc. and several low level controllers are responsible for attitude and altitude stabilization. Results of several simulations and real flight tests are provided along with flight data to show performance of the developed UAV.

1. Introduction

Multi-purpose, compact unmanned aerial vehicles have been gaining remarkable capabilities in the last decades. They are important due to their abilities to replace manned aircrafts in many routine and dangerous missions, and to reduce costs of many aerial operations [1,2]. These aerial robots can be utilized in a variety of civilian missions such as surveillance in disasters, traffic monitoring, law enforcement and power line maintenance [3–7]. They are already being benefitted in military applications such as intelligence, surveillance, target acquisition, reconnaissance and aerial attacks [3,8–12]. These application areas lead to more advanced research for increasing the level of autonomy and reducing the size of UAVs. UAVs can be classified into three main categories: fixed-wing UAVs, rotary-wing UAVs, and hybrid design UAVs.

Fixed wing UAVs constitute the richest group among these categories both in terms of research and utilization. They are able to fly for long duration at high speeds and their design is simple in comparison with the other types of UAVs. These advantages lead to a broad range of fixed wing UAV designs from RQ-4 Global Hawk with 39.8 m wingspan to AeroVironment Wasp with 72 cm wingspan. However, these UAVs suffer from the requirement of runways or additional launch and recovery equipment for takeoff and landing. Rotary wing UAVs, on the other hand, are advantageous since they do not require any infrastructure for takeoff and landing. They also do not need any forward airspeed for flight and maneuvering, which makes them useful particularly in urban areas and indoors. This leads to a large variety of rotary wing UAVs ranging from Boeing A160 Hummingbird with 2948 kg flight weight to Seiko–Epson μ Flying Robot with only 12.3 g flight weight. But they are mechanically complex and have low flight speeds and durations.

Hybrid design UAVs join the vertical flight capabilities of rotary wing UAVs with the high speed long duration flight capabilities of fixed wing UAVs. Despite their increased mechanical complexity and more difficult control, they are very desirable for their ability to act like both fixed wing and rotary wing UAVs, since this ability is very useful in various missions. Among these hybrid designs, tilt-rotor UAVs constitute an attractive research area due to their stability, energy efficiency and controllability [13,14]. A large proportion of the research on these vehicles are on dual tilt-rotors such as Bell Eagle Eye, Smart UAV of KARI and BIROTAN [15] and dual tilt-wings such as HARVee [16] and the UAV of Universita di Bologna. The dual rotor UAVs generally require cyclic control on propellers, which adds to the mechanical complexity, for stabilization and maneuvering. To solve this problem there are also studies on quad tilt-wing UAVs such as QUX-02 of Japan Aerospace Exploration Agency and QTW of Chiba University and G.H. Craft [17,18].

In this work, a novel electric powered quad tilt-wing UAV (SUAVI: Sabanci University Unmanned Aerial VehIcle) is presented. It has four rotors that are mounted on the four wings. The wings, together with the rotors, are tilted between vertical and horizontal configurations to accomplish vertical and horizontal flights. It is similar to a quadrotor helicopter in vertical and a tandem wing airplane in horizontal flight modes. Electric motors for propulsion are

* Corresponding author.
E-mail addresses: cetinsoy@sabanciuniv.edu (E. Cetinsoy), serhatdikyar@sabanciuniv.edu (S. Dikyar), chancer@sabanciuniv.edu (C. Hancer), kaanoner@sabanciuniv.edu (K.T. Oner), efesirimoglu@sabanciuniv.edu (E. Sirimoglu), munel@sabanciuniv.edu (M. Unel), aksit@sabanciuniv.edu (M.F. Aksit).

0957-4158/$ - see front matter © 2012 Elsevier Ltd. All rights reserved.
http://dx.doi.org/10.1016/j.mechatronics.2012.03.003

placed on the leading edges of each wing: the motors lift SUAVI when the wings are vertical and they provide forward thrust for horizontal motion when the wings are tilted. SUAVI can track a route autonomously utilizing GPS data and can be controlled manually when needed. It has an onboard surveillance camera to transmit images to the ground station.

To achieve long duration flight in various missions, optimum selection of wing profiles and the body shape is required. The wing profile is chosen according to the lift-drag requirements of SUAVI and the body shape is determined by taking both the utilization and the aerodynamic efficiency into account. Mechanical design of SUAVI is carried out by considering weight limitation, strength and utilization of the aircraft. To obtain a prototype that is both lightweight and strong against flight and landing forces, the body is designed to be produced using carbon composite material. For increasing the strength, a carbon composite pipe chassis is utilized as a backbone for the aircraft. This chassis supports the lightweight skins of the fuselage and wings. To provide easy assembly of the wings to the body and smooth wing tilting operation, needle bearing supported all aluminum wing tilting mechanisms are utilized in the wing-body joints.

To develop flight control system, a full dynamical model is derived using Newton–Euler formulation. A hierarchical control system, including a high level controller that is responsible for the switching of the low-level controllers into the closed-loop system, generating GPS based attitude references and performing safety checks, and low level controllers for stabilization of the aerial vehicle, is designed and implemented. In line with the control system hierarchy, vertical, transition and horizontal mode flight controllers are developed. In order to design flight controllers, the dynamics of the aerial vehicle is divided into two subsystems, namely position and attitude subsystems. PID controllers are designed for position subsystem that has slower dynamics when compared with the attitude subsystem. Reference attitude angles are computed by utilizing the dynamic inversion method and the virtual control inputs generated by position controllers. Attitude subsystem is linearized by feedback linearization and reference angles computed by position subsystem are used by the PID type controllers that are designed for attitude subsystem. The proposed control architecture is implemented in hardware using various sensors, actuators, a Gumstix microcomputer and several microcontrollers.

There are several unique features that distinguishes this work from the other quad tilt-wing UAV designs reported in the literature. When compared with the QUX-02 of Japan Aerospace Exploration Agency [17], SUAVI is a more compact platform with 1 m versus 1.1 m fuselage length and 1 m versus 1.38 m wingspan. It is approximately 30% heavier, but it is designed to achieve nearly half hour vertical and 1 h horizontal flights, whereas the reported flights of the QUX-02 do not exceed 16 min including horizontal flight modes. SUAVI utilizes the same wings at the front and the rear to simplify the prototyping and increase the part commonality. Its aerodynamic characterization is carried out by considering different angle of attacks and motor thrusts at front and rear wings for the nominal flight. On the other hand, in QUX-02 the rear wings have larger wing spans than the front wings for the utilization of similar wing angle of attacks at front and rear wings. SUAVI is a mechanically optimized carbon composite UAV with a complex onboard control system and full and semi-autonomous flight capabilities, while QUX-02 is a preliminary work produced using balsa wood for the feasibility determination of quad tilt-wing configuration with a simple control system and semi-autonomous flight.

When compared with the QTW of G.H. Craft [18], SUAVI is clearly a more compact and light-weight platform with 1 m versus 1.61 m fuselage length, 1 m versus 1.34 m wingspan and 4.46 kg versus 24 kg weight. QTW is nearly four times heavier than SUAVI and is designed for high speed flights (up to 150 km/h) in horizontal flight, whereas SUAVI is optimized for horizontal flight at lower speeds (up to 60 km/h) and also for indoor flights. Additionally, for research on such aircrafts, SUAVI offers a low cost platform when compared with the QTW and it can be easily transported to the test field with its easily detachable wings, whereas QTW is a large aircraft with wings that are built in one piece. Furthermore, SUAVI is designed as a quad tilt-wing aircraft with clock-wise and counter clock-wise propellers for the balancing of yaw moments of the rotating propellers and yaw control in vertical flight mode. QUX-02 and QTW UAVs, on the other hand, utilize flaperons on the trailing edges of the wings. To the best of our knowledge, this work also provides the first full nonlinear dynamical model for a quad tilt-wing UAV.

The rest of the paper is organized as follows: in Section 2 the design of SUAVI including aerodynamic and mechanical design, and prototyping is presented. The flight control system design is detailed in Section 3. Control system hardware is explained in Section 4, and simulation and real flight test results are provided in Section 5. Finally, the paper is concluded with some remarks in Section 6 and some future work is indicated.

2. Design and prototyping

The design of SUAVI is shaped based on the operational requirements. The aircraft is aimed to operate in surveillance missions such as traffic control, security missions, and disasters including indoor-outdoor fires, floods, earthquakes. To satisfy the requirements of these tasks, it is planned to takeoff and land vertically, hover and fly in an airspeed range of 0–60 km/h for both stationary and in-motion surveillance. The vertical flight endurance of the aircraft is planned to reach half hour whereas its horizontal flight endurance is to exceed 1 h. SUAVI is also aimed to be compact for indoor surveillance and mechanically simple for operational reliability. To meet such flight capabilities with these features, SUAVI is designed as an electric powered quad tilt-wing air vehicle where four motors are mounted on the mid-span leading-edges of the wings and the wings are tilted in horizontal-vertical position range. Motors rotate constant pitch propellers for mechanical simplicity, altering thrust through RPM change and the electric source is high capacity Li–Po batteries. In this design, wings are tilted to vertical position to form a quad-rotor helicopter using only motor thrusts for lift on vertical takeoff, landing and hovering. When horizontal flight is required, wings are tilted gradually to the appropriate angles of the desired speed and motor thrusts are adjusted accordingly. At high speeds, wings are tilted to nearly-horizontal position to generate lift and motors generate forward thrust, forming a tandem wing airplane. The design length and wingspan of the aircraft are both 1 m and design weight is 4.5 kg.

2.1. Aerodynamic design

The aim of the aerodynamic design is to choose the most appropriate propulsion system and to minimize air drag while generating sufficient lift for flight with the least complicated and most lightweight structure.

The criteria in the selection of the motors are to produce the required shaft power, to be lightweight and mechanically durable, and to have effective cooling for long duration flights. Based on these criteria, Great Planes Rimfire 42-40-800 motor is chosen as the source of propulsion. It delivers up to 1.6 kg of static thrust with appropriate propellers when powered with 11.1 V batteries and is allowed to draw 32 A maximum current. For the decision on the propeller type to be used, several suggested APC electric motor propellers from size $11'' \times 8''$ to $16'' \times 5''$ (former number: diameter in inch, latter number: pitch in inch) are tested on the

Please cite this article in press as: Cetinsoy E et al. Design and construction of a novel quad tilt-wing UAV. Mechatronics (2012), http://dx.doi.org/10.1016/j.mechatronics.2012.03.003

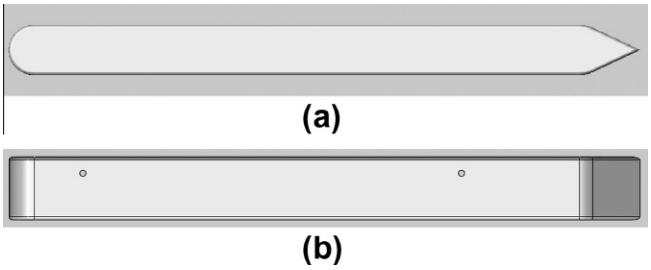

Fig. 1. Top (a) and side (b) views of the fuselage.

thrust test bench with the selected motor. The motor-propeller couples are tested for maximum thrust and current for nominal thrust per motor during hover. As a result of these tests, the appropriate propeller size is chosen as $14'' \times 7''$. When the maximum speed potentials of these propellers are tested, it is observed that $14'' \times 7''$ propeller is sufficient to cope with the drag at 60 km/h airspeed. The propulsion system is powered by 30 Ah Li–Po batteries that are placed in the wings.

The fuselage is designed as a rectangular prism with rounded nose section and a back section with gradually decreasing thickness for high aerodynamic efficiency. When viewed from the top of the air vehicle, the fuselage resembles a symmetrical wing with long straight sides (Fig. 1a). One advantage of this shape is the low drag coefficient due to its resemblance to a water drop. Another advantage is that the straight sides behave as flow boundaries to prevent additional loss due to spanwise flows at the roots of the wings (Fig. 1b).

The shape of the wings is selected by taking the speed range, wing span limitation, efficiency and interactions with the fuselage into consideration. To determine the fuselage dimensions, chord length, camber ratio and the thickness of the airfoil, various air flow simulations are performed in *ANSYS*® environment. The effects of the slipstream velocities of the propellers are also employed since the rotors have great effect on the overall behavior of the wings. For these simulations, the 3D CAD model of SUAVI is drawn in *SolidWorks*® and imported into the ANSYS air flow simulation environment. The boundary conditions are symmetry at the vertical symmetry plane between left and right halves of the aircraft, zero air speed on the surfaces of the UAV due to the stiction, tested air speed at the incoming side of the closed volume and ambient air pressure at the outgoing side of the closed volume.

In these air flow simulations, it is observed that using relatively long chord length with large winglet instead of high wing thickness is more preferable to increase efficiency. This is due to the fact that at high angle of attacks large chord length supplies large inclined surface against the air flow and at high speeds thicker wing causes more drag. In the literature, it is known that thinner and less cambered wings suffer from leading edge separation at lower angle of attacks, which causes stall [19]. However, wings of SUAVI are almost fully submerged in the slipstream of the propellers and the high speed slipstream prevents the air separation even at high angle of attacks and supplies additional lift.

Due to the low aspect ratio (AR = 4) and rectangular planform, the wings of the air vehicle have tendency to have severe spanwise air flow, especially at high angle of attacks (Fig. 2a). This spanwise air flow reduces the efficiency of the wings by generating wing tip

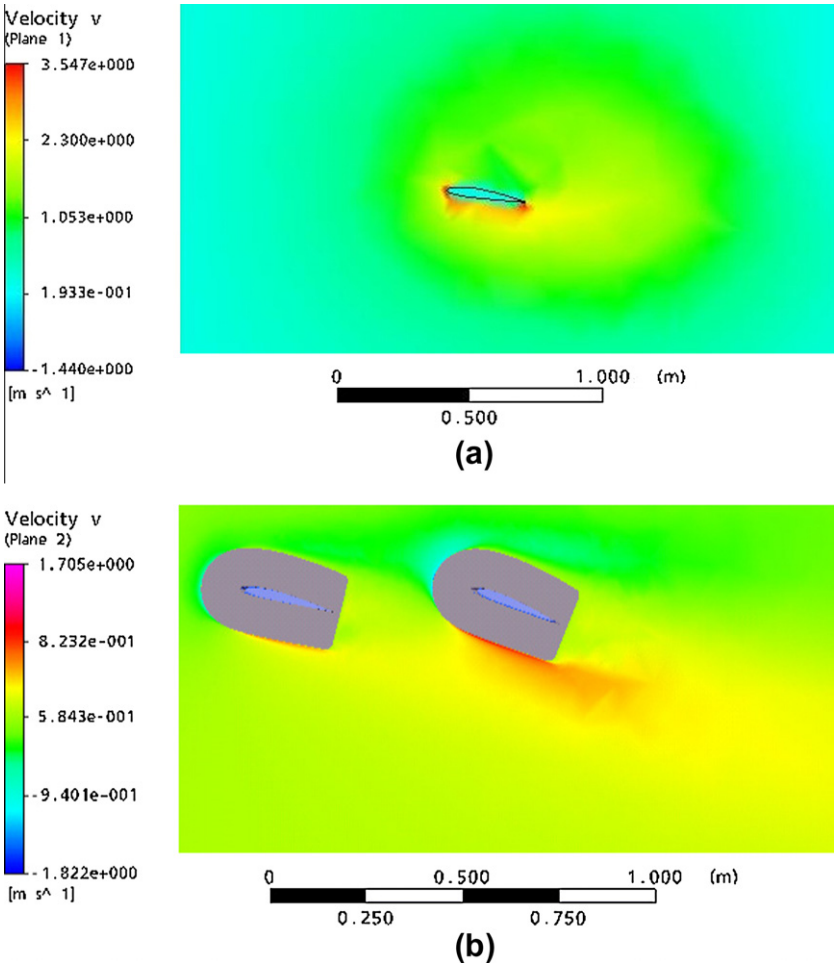

Fig. 2. Spanwise airflow without winglets (a) and reduction of the spanwise airflow by winglets (b).

Please cite this article in press as: Cetinsoy E et al. Design and construction of a novel quad tilt-wing UAV. Mechatronics (2012), http://dx.doi.org/10.1016/j.mechatronics.2012.03.003

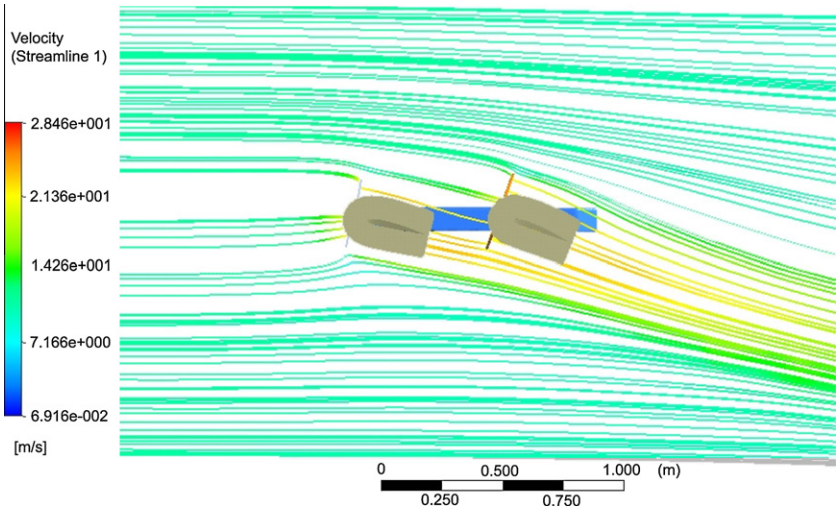

Fig. 3. Streamlines showing the downwash and its effect on the rear wing.

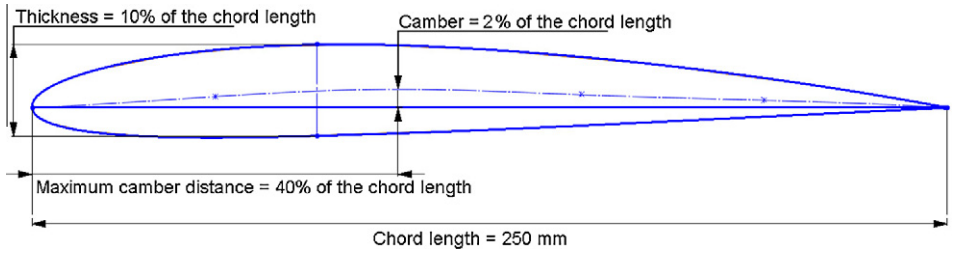

Fig. 4. NACA 2410 airfoil.

vortex and reducing pressure difference between the upper and lower surfaces. To cope with this problem, large winglets are joined to the wing tips (Fig. 2b). From the ANSYS air flow simulations of the air vehicle with consecutive wings, it is noticed that the lift of rear wings is negatively affected by the downwash of the front wings (Fig. 3), which imposes imbalance in transition and horizontal flight modes since the air vehicle's center of mass is located between the lift centers of the consecutive wings. This downwash decreases the rear wings' effective angle of attack and the downwash angle increases with the front wing angles [19–21]. To solve this problem without complicating the design and production, the front and rear wings are located at the same vertical level and the rear wings are used with higher angle of attack.

As a result of extensive simulations, NACA 2410 airfoil with 25 cm chord length is selected to be sufficient both for generating the required lift and for constraining the air drag at a considerable level (Fig. 4). This airfoil has a maximum camber line to mean line distance of 2% of the chord length at a 40% chord length distance behind the leading edge and a maximum thickness of 10% chord length.

According to the simulations, SUAVI can fly most economically at around 40 km/h air speed with 10.5° front wing angle of attack and 12.5° rear wing angle of attack, while it can speed up to 60 km/h with 2° front wing angle of attack and 3.7° rear wing angle of attack. At 40 km/h, without any propeller slipstream, the risk of separation exists. However, the slipstream of the motors increases the airspeed on the wings with additional parallel to chord air flow and prevents any separation on the wings.

Fig. 5. Half model in the wind tunnel.

For the experimental aerodynamic characterization of SUAVI, wind tunnel tests are performed. A half model of SUAVI is designed and produced with a half aluminum fuselage and prototype wings (Fig. 5).

In these tests the main focus is to determine the wing angle of attacks and motor thrust references for nominal flight on the entire

Please cite this article in press as: Cetinsoy E et al. Design and construction of a novel quad tilt-wing UAV. Mechatronics (2012), http://dx.doi.org/10.1016/j.mechatronics.2012.03.003

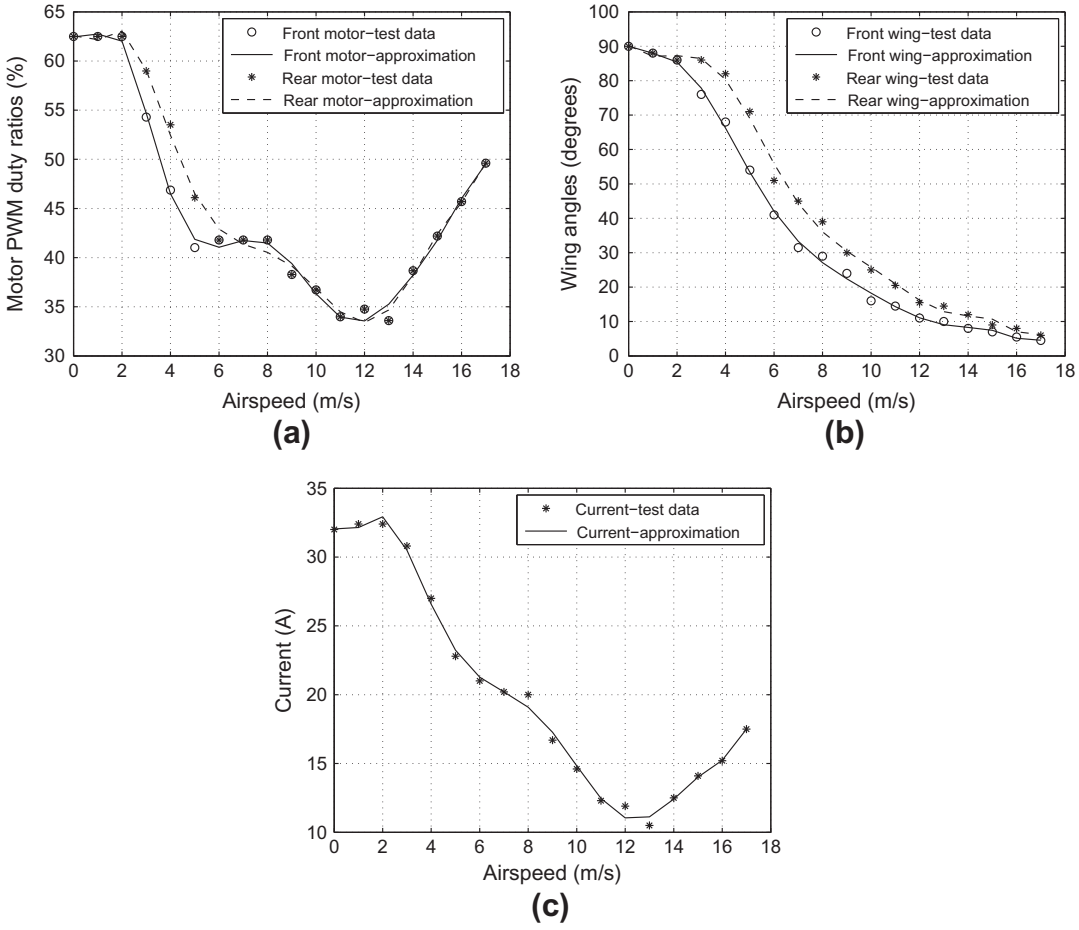

Fig. 6. Motor PWM duty ratios (a), wing angles (b) and current drawn by the half model for steady flight at various speeds.

Table 1
Look-up table for motor PWM percentages, wing angle of attacks and current drawn by two motors on the half model for nominal flight.

Air speed (m/s)	Front motor (%)	Rear motor (%)	Front wing angle (°)	Rear wing angle (°)	Current (A)
0	62.5	62.5	90.0	90.0	32.0
1	62.5	62.5	88.0	88.0	32.4
2	62.5	62.5	86.0	86.0	32.4
3	54.3	59.0	76.0	86.0	30.8
4	46.9	53.5	68.0	82.0	27.0
5	41.0	46.1	54.0	71.0	22.8
6	41.8	41.8	41.0	51.0	21.0
7	41.8	41.8	31.5	45.0	20.2
8	41.8	41.8	29.0	39.0	20.0
9	38.3	38.3	24.0	30.0	16.7
10	36.7	36.7	16.0	25.0	14.6
11	34.0	34.0	14.5	20.5	12.3
12	34.8	34.8	11.0	15.5	11.9
13	33.6	33.6	10.0	14.5	10.5
14	38.7	38.7	8.0	12.0	12.5
15	42.2	42.2	7.0	9.0	14.1
16	45.7	45.7	5.5	8.0	15.2
17	49.6	49.6	4.5	6.0	17.5

speed range. It is found that at high and low speeds, angle of attacks and motor throttle settings of front and rear wings are similar and they differ at the moderate speed range due to the downwash effect of the front wing (Fig. 6a and b). It is also found that the most economical flight speed of SUAVI is approximately 12 m/s that corresponds to 43.2 km/h (Fig. 6c), which is close to what was predicted by ANSYS simulations. The wing angle of attacks, motor PWMs and current requirements of the half model are tabulated in Table 1. This table is used as a look-up table by the control system in the transition flights.

In light of Table 1, two motors on the half model draw 32 A in vertical flight (wing angles are both 90°) and 10.5 A in the most economical flight speed (13 m/s) in horizontal flight (wing angles are 10° and 14.5°). Therefore, the aerial vehicle with four motors

Please cite this article in press as: Cetinsoy E et al. Design and construction of a novel quad tilt-wing UAV. Mechatronics (2012), http://dx.doi.org/10.1016/j.mechatronics.2012.03.003

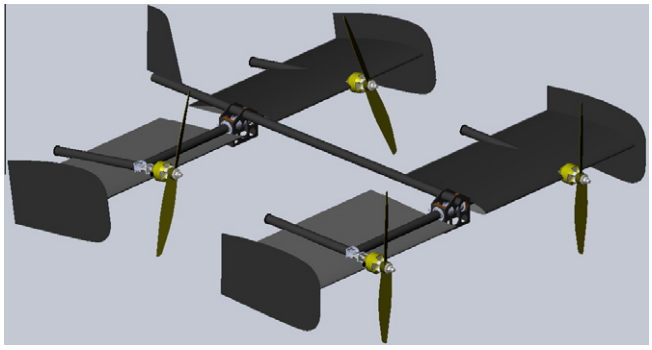

Fig. 7. CAD model of the body with partial covering for demonstrating the chassis.

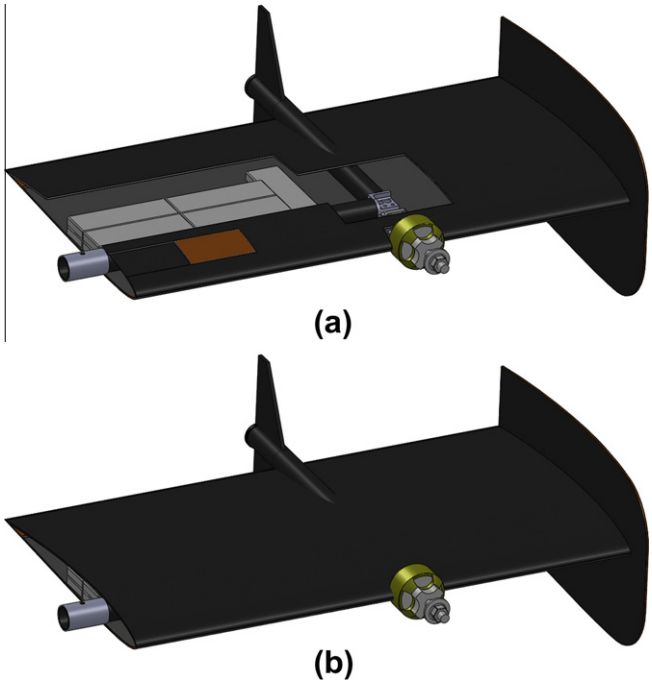

Fig. 8. CAD model of the wing with regionally cut upper skin to reveal the details (a) and with its final shape (b).

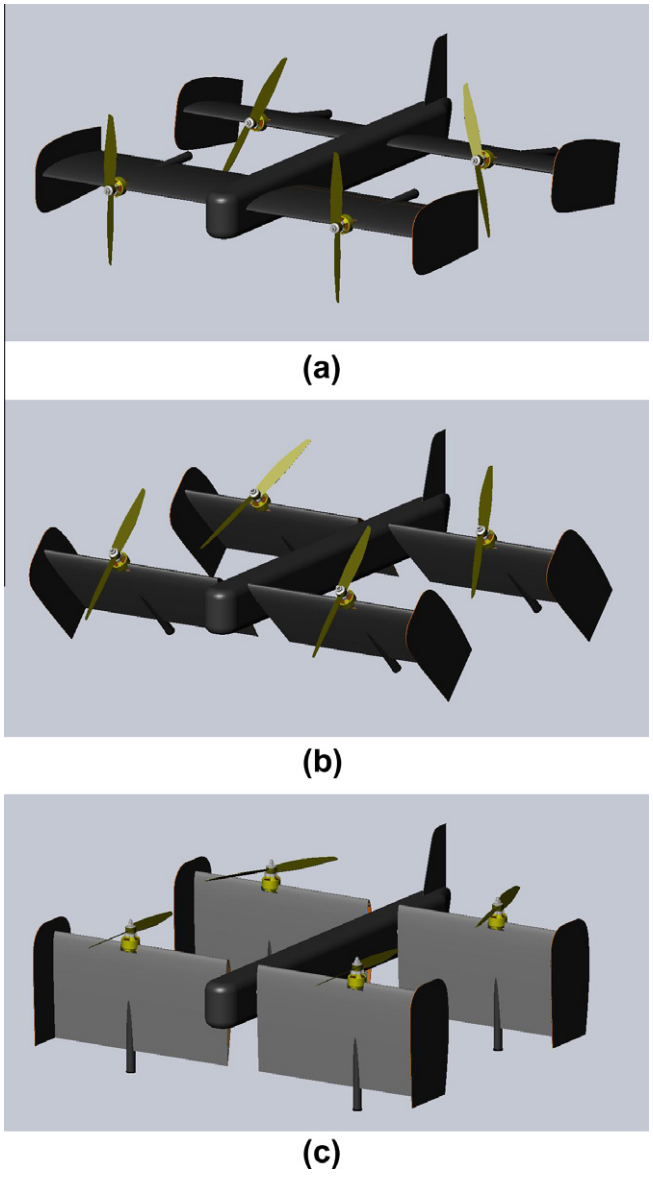

Fig. 10. CAD model of SUAVI in horizontal (a), transition (b) and vertical (c) flight modes.

consumes 64 A in vertical and 21 A in horizontal flight. Thus, in order to keep the aerial vehicle in hover for half an hour, 32 Ah battery capacity is required. Since the Li–Po battery used on the prototype has 30 Ah capacity, approximately half an hour vertical flight is predicted. Additionally, four motors require 21 Ah battery capacity for 1 h horizontal flight. With 30 Ah battery capacity, more than 1 h flight is expected.

2.2. Mechanical design

The main goal of the mechanical design is to obtain the most lightweight structure that is capable of withstanding the possible loadings in vertical, horizontal and transition flight modes. To achieve this, carbon fiber reinforced plastic, a material that is known to be the best in terms of strength/weight ratio, is determined to be

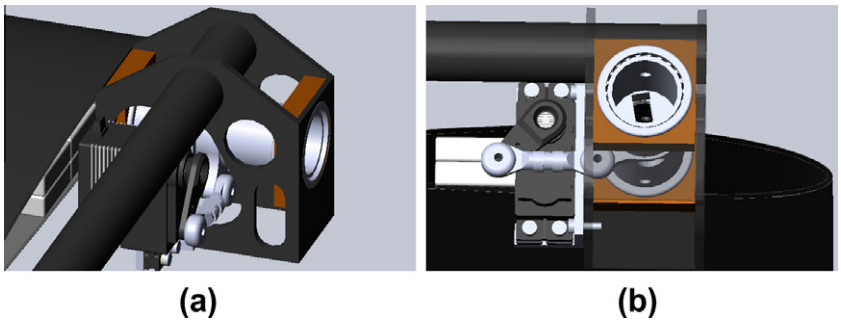

Fig. 9. CAD model of the wing-tilting mechanism-carbon pipe connection (a) and wing-tilting mechanism detail (b).

Please cite this article in press as: Cetinsoy E et al. Design and construction of a novel quad tilt-wing UAV. Mechatronics (2012), http://dx.doi.org/10.1016/j.mechatronics.2012.03.003

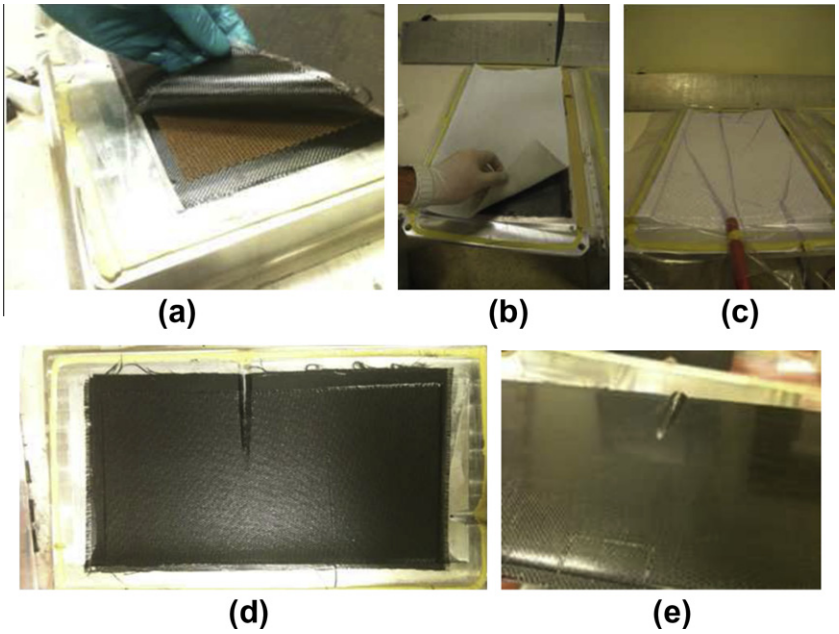

Fig. 11. Hand lay-up (a), vacuum-bagging (b and c), cured skin (d) and the cutting marks on the skins (e).

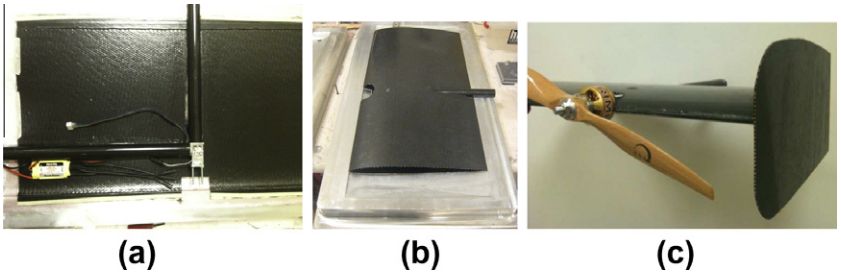

Fig. 12. Inner parts being attached to the lower wing skin (a), joining of the upper skin onto the wing (b) and joining of the winglet (c).

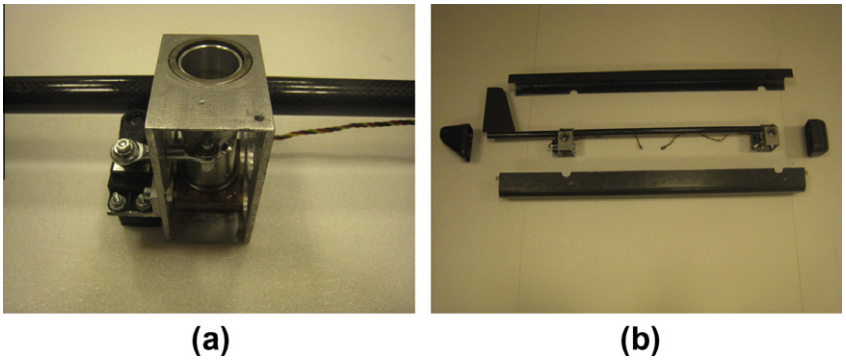

Fig. 13. Wing tilting mechanism (a), the assembly of the fuselage skeleton (b).

the production material of SUAVI. To improve the durability in compression loading, usage of sandwich structure on the entire body is preferred. In this sandwich structure, lightweight Aramid honeycomb core material is surrounded by carbon fiber cloth on both sides. This structure makes the skins of the UAV to perform like an I-beam, in which the strong material is kept at outer sides to increase the second moment of inertia and low-density material is kept inside just to keep the outer sides parallel to and apart from each other. By this way, the skins of the UAV can be produced lightweight and still strong, even against bending and compression.

A carbon composite tube chassis is embedded in the design as a strong skeleton for carrying the loads and reducing the weight of the skins as much as possible (Fig. 7). This chassis extends from the fuselage to the tips of the landing arms.

The sandwich structure that carries the stresses on the wings transmits the generated forces to the carbon composite tube wing spars. Likewise, the aluminum elbow connection parts connect the landing arms and the electric motors to the spars to transmit the landing impact and motor thrusts to the fuselage through a durable and stiff chassis. The spars are attached to the inner walls of both

Please cite this article in press as: Cetinsoy E et al. Design and construction of a novel quad tilt-wing UAV. Mechatronics (2012), http://dx.doi.org/10.1016/j.mechatronics.2012.03.003

the upper and lower wing surfaces, providing nearly all stresses on the wing surfaces to be in tension and transmitted continuously to the spars (Fig. 8a).

The motors are mounted nearly at the mid-span of the wings and the landing arms are placed directly behind the motors to minimize possible bending moments observed during touchdown. There are tail-fin alike extensions designed for the tips of the landing arms to prevent the failing of wing tilting servos to keep the wings vertical during possible problematic touchdowns with some forward motion (Fig. 8b). Additionally, the Li–Po batteries are located in the wings to keep the rolling inertia near to pitching inertia and at a reasonable level for better stability characteristics.

To keep the fuselage both lightweight and stiff against bending and torsion, the front and rear wing tilting mechanisms are also connected through the same type carbon composite tube (Fig. 9a and b). This tube ends at the front wing tilting mechanism, whereas it extends further beyond the rear wing tilting mechanism to provide a stiff support for the vertical stabilizer of the aerial vehicle. This tube is fixed to the outer static structure of the wing-tilting mechanism (Fig. 9a and b). This outer static structure is charged to carry the high torque servo near the rotating shaft and the needle bearings on which the shaft is rotating, transmit forces from the wings to the body, and carry the aerodynamic cover.

The servo rotates the shaft, on which the wing spars are fixed, through a parallel mechanism with around 100° tilting range. The wing spars are inserted into the shaft and then screwed to it on matching holes with setscrews to keep the wings at correct place and angle. An important detail on this system is the thin rings stuck on the tips of the wing spars. The outer diameter of the carbon composite tubes vary in the order of some 0.1 mm.

Finally, it is useful to pass the cabling between the wings and the fuselage through the carbon composite spars and the rotating shafts in the wing tilting mechanism (See Fig. 14a in Section 2.3). Otherwise, these cables are damaged by the carbon composite skin of the fuselage after several numbers of vertical–horizontal transitions during the operation of SUAVI. There are also four aerodynamic cover parts produced from sandwich structured carbon composite material with aramid honeycomb core: the nose, the stern, the lower mid part and the upper mid part. The resulting CAD model of the SUAVI is depicted in Fig. 10.

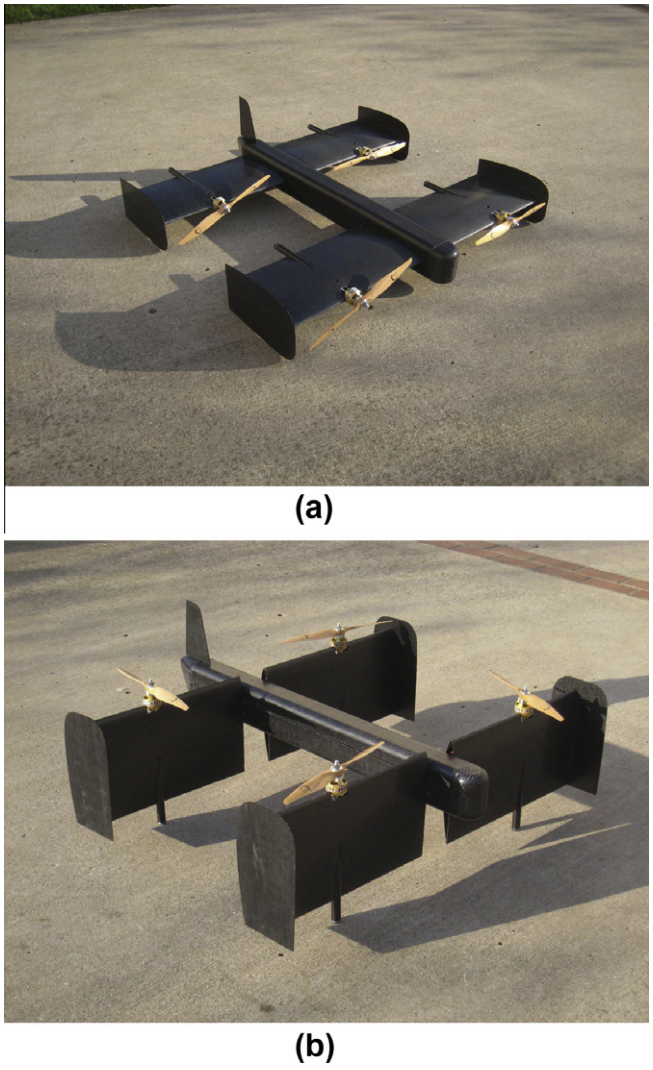

Fig. 15. SUAVI prototype in horizontal (a) and vertical (b) flight modes.

2.3. Prototyping

For prototyping, sandwich structured carbon composite material with Aramid honeycomb core and 90 g/m^2 0–90 plain wave carbon cloth is utilized. The production of the skins begins with the hand lay-up of the impregnated carbon cloth and honeycomb core (Fig. 11a). They are cured through the vacuum bagging process (Fig. 11b and c). The cured parts are extracted from the mold (Fig. 11d) and the grooves are cut for the motor placement (Fig. 11e).

For the assembly of the wings, a preassembled wing spar, elbow connector and landing arm group with the flight-ready cabling of motor throttle pulse and battery power transmission is fixed on the lower wing skin on the mold with epoxy (Fig. 12a). After the fixing of the upper skin of the wing (Fig. 12b), the assembly of

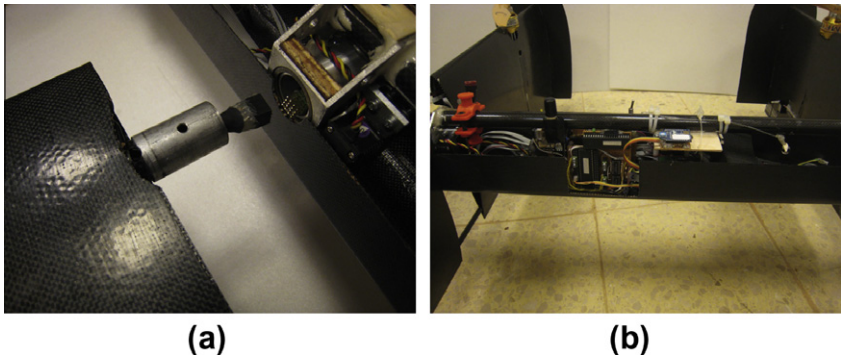

Fig. 14. Cable connections during the assembly (a) and addition of electronic control system (b).

Please cite this article in press as: Cetinsoy E et al. Design and construction of a novel quad tilt-wing UAV. Mechatronics (2012), http://dx.doi.org/10.1016/j.mechatronics.2012.03.003

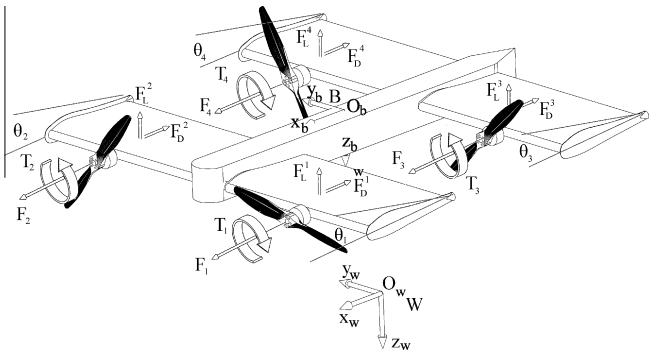

Fig. 16. External forces and moments acting on the vehicle.

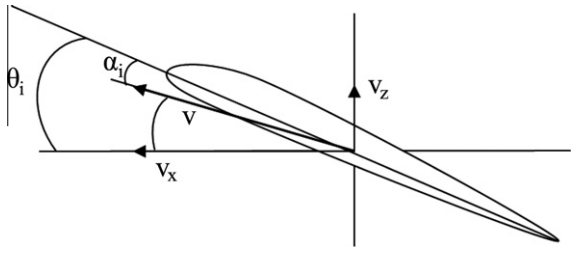

Fig. 17. Effective angle of attack α_i.

the wing is concluded with the joining of the motor and the winglet (Fig. 12c).

The assembly of the fuselage begins with the assembly of the wing tilting mechanisms. The needle bearings and the high torque wing tilting servo are joined to each casing of the tilting mechanism and the connection between the servo and the wing rotating shaft is established via the pushrod (Fig. 13a). The fuselage is completed with the assembly of the wing tilting mechanisms and the vertical stabilizer on the carbon composite tube (Fig. 13b).

With the addition of the electronic control system (Fig. 14), SUAVI becomes ready for flight (Fig. 15a and b). The ready for flight weight of the prototype is 4460 g, in which the body without electronic systems, batteries and motors weighs only 626 g, which is remarkably low when the size, rigidity and the weight of the aluminum mechanisms are taken into account.

3. Flight control system design

A flight control system is required to fly the air vehicle in fully or semi autonomous mode. To achieve accurate trajectory tracking, first a full dynamical model of the aerial vehicle is derived that includes the effects of the propulsion system, the aerodynamic forces and the disturbances. A hierarchical control system incorporating both high-level and low-level control is designed and implemented.

3.1. Dynamical Model

SUAVI is a highly coupled nonlinear system that changes the flight mode to change the horizontal flight speed. This also alters the control laws and the model significantly due to the fact that the reactions of the air vehicle to motor thrusts and wing angle of attacks change significantly with the flight mode.

Assuming the aerial vehicle as a 6 DOF rigid body, the dynamical model of SUAVI is derived using Newton–Euler formulation.

Two reference frames are utilized in the mathematical modeling of the aerial vehicle. They are the World frame W:(O_w, x_w, y_w, z_w) and the Body frame B:(O_b, x_b, y_b, z_b). In the earth fixed inertial reference frame (world frame), x_w is directed northwards, y_w is directed eastwards, z_w is directed downwards and O_w is the origin of the world frame. Similarly, in the body frame, x_b is directed to the front of the vehicle, y_b is directed to the right of the vehicle, z_b is directed downwards and O_b is the origin at the center of mass of the aerial vehicle.

The position and linear velocity of the vehicle's center of mass in the world frame are expressed as

$$P_w = [X, Y, Z]^T, \quad V_w = \dot{P}_w = [\dot{X}, \dot{Y}, \dot{Z}]^T \tag{1}$$

Vehicle's attitude and its time derivative in the world frame are defined as

$$\alpha_w = [\phi, \theta, \psi]^T, \quad \Omega_w = \dot{\alpha}_w = [\dot{\phi}, \dot{\theta}, \dot{\psi}]^T \tag{2}$$

where ϕ, θ and ψ are roll, pitch and yaw angles, respectively. The orientation of the body frame with respect to the world frame is expressed by the rotation matrix

$$R_{wb}(\phi, \theta, \psi) = \begin{bmatrix} c_\psi c_\theta & s_\phi s_\theta c_\psi - c_\phi s_\psi & c_\phi s_\theta c_\psi + s_\phi s_\psi \\ s_\psi c_\theta & s_\phi s_\theta s_\psi + c_\phi c_\psi & c_\phi s_\theta s_\psi - s_\phi c_\psi \\ -s_\theta & s_\phi c_\theta & c_\phi c_\theta \end{bmatrix} \tag{3}$$

The transformation of linear velocities between the world and the body frames is given as

$$V_b = \begin{bmatrix} v_x \\ v_y \\ v_z \end{bmatrix} = R_{wb}^T(\phi, \theta, \psi) \cdot V_w = R_{bw}(\phi, \theta, \psi) \cdot V_w \tag{4}$$

The relation between the angular velocity of the vehicle and the time derivative of the attitude angles is given by the following transformation

$$\Omega_b = \begin{bmatrix} p \\ q \\ r \end{bmatrix} = \mathbb{E}(\alpha_w) \cdot \Omega_w = \mathbb{E}(\alpha_w) \cdot \begin{bmatrix} \dot{\phi} \\ \dot{\theta} \\ \dot{\psi} \end{bmatrix} \tag{5}$$

where $\mathbb{E}$ is the velocity transformation matrix [22,23] and defined as

$$\mathbb{E}(\alpha_w) = \begin{bmatrix} 1 & 0 & -s_\theta \\ 0 & c_\phi & s_\phi c_\theta \\ 0 & -s_\phi & c_\phi c_\theta \end{bmatrix} \tag{6}$$

In this equation $c_{(.)}$ and $s_{(.)}$ denotes cos(.) and sin(.), respectively. Inverse of the velocity transformation is denoted as $\mathbb{B}(\alpha_w)$ and implies

$$\Omega_w = \mathbb{E}^{-1}(\alpha_w) \cdot \Omega_b = \mathbb{B}(\alpha_w) \cdot \Omega_b \tag{7}$$

Since the aerial vehicle is assumed as a rigid body, its dynamics can be written as

$$\begin{bmatrix} mI & 0 \\ 0 & I_b \end{bmatrix} \begin{bmatrix} \dot{V}_w \\ \dot{\Omega}_b \end{bmatrix} + \begin{bmatrix} 0 \\ \Omega_b \times (I_b \Omega_b) \end{bmatrix} = \begin{bmatrix} F_t \\ M_t \end{bmatrix} \tag{8}$$

where the subscripts w and b express the vector and matrix quantities in world and body frames, respectively. m denotes the mass and I_b denotes the vehicle's inertia matrix. I and 0 are 3×3 identity and zero matrices, respectively. The left hand side of (8) is standard for many aerial vehicle types, however the total force and moment terms, F_t and M_t, are different for different aerial vehicles.

Note that for a quad tilt-wing aerial vehicle, the terms F_t and M_t are functions of the motor thrusts, forces on the wings and the fuselage, and also the wing angle of attacks. These forces and torques are depicted in Fig. 16.

The total external force F_t consists of the motor thrusts F_{th}, aerodynamic forces on the wings F_w, gravity force on the vehicle F_g and external disturbances such as winds and gusts F_d. These forces are

Please cite this article in press as: Cetinsoy E et al. Design and construction of a novel quad tilt-wing UAV. Mechatronics (2012), http://dx.doi.org/10.1016/j.mechatronics.2012.03.003

expressed in the body frame and have to be transformed by R_{wb} to be expressed in the world frame as follows

$$F_t = R_{wb}(F_{th} + F_w + F_g + F_d) \tag{9}$$

where

$$F_{th} = \begin{bmatrix} c_{\theta_1} & c_{\theta_2} & c_{\theta_3} & c_{\theta_4} \\ 0 & 0 & 0 & 0 \\ -s_{\theta_1} & -s_{\theta_2} & -s_{\theta_3} & -s_{\theta_4} \end{bmatrix} \begin{bmatrix} k\omega_1^2 \\ k\omega_2^2 \\ k\omega_3^2 \\ k\omega_4^2 \end{bmatrix}$$

$$F_w = \begin{bmatrix} (F_D^1 + F_D^2 + F_D^3 + F_D^4) \\ 0 \\ (F_L^1 + F_L^2 + F_L^3 + F_L^4) \end{bmatrix}$$

and

$$F_g = \begin{bmatrix} -s_\theta \\ s_\phi c_\theta \\ c_\phi c_\theta \end{bmatrix} mg$$

In these equations, θ_i denotes wing angles with respect to the body. Note that the motor thrusts are modeled as

$$F_i = k\omega_i^2 \tag{10}$$

where ω_i is the rotor rotational speed.

To simplify the design of the aerial vehicle, left and right wings both at the back and at the front are tilted together, leading to the relations $\theta_1 = \theta_2$ and $\theta_3 = \theta_4$. The lift forces $F_L^i(\theta_i, v_x, v_z)$ and the drag forces $F_D^i(\theta_i, v_x, v_z)$ are functions of linear velocities v_x and v_z, and the wing angle of attacks θ_i, namely

$$\begin{bmatrix} F_D^i \\ 0 \\ F_L^i \end{bmatrix} = R(\theta_i - \alpha_i) \begin{bmatrix} -\frac{1}{2} c_D(\alpha_i) \rho A v_\alpha^2 \\ 0 \\ -\frac{1}{2} c_L(\alpha_i) \rho A v_\alpha^2 \end{bmatrix} \tag{11}$$

where

$$v_\alpha = \sqrt{v_x^2 + v_z^2}$$
$$\alpha_i = \theta_i - (-atan2(v_z, v_x))$$

In these equations, ρ is the air density, A is the wing planform area, v_α is the airflow velocity and α_i is the effective angle of attack of the wing with respect to the air flow as depicted in Fig. 17. $R(\theta_i - \alpha_i)$ is the rotation matrix for the rotation around y axis that decomposes the forces on the wings onto the body axes. The total moment M_t consists of the moments created by the rotors M_{th}, moments created by the aerodynamic forces produced by the wings M_w, moments created by the gyroscopic effects of the propellers M_{gyro} and moments due to the external disturbances M_d; i.e.

$$M_t = M_{th} + M_w + M_{gyro} + M_d \tag{12}$$

where

$$M_{th} = l_s \begin{bmatrix} s_{\theta_1} - \frac{\lambda_1}{l_s} c_{\theta_1} & -s_{\theta_2} - \frac{\lambda_2}{l_s} c_{\theta_2} & s_{\theta_3} - \frac{\lambda_3}{l_s} c_{\theta_3} & -s_{\theta_4} - \frac{\lambda_4}{l_s} c_{\theta_4} \\ \frac{l_l}{l_s} s_{\theta_1} & \frac{l_l}{l_s} s_{\theta_2} & -\frac{l_l}{l_s} s_{\theta_3} & -\frac{l_l}{l_s} s_{\theta_4} \\ c_{\theta_1} + \frac{\lambda_1}{l_s} s_{\theta_1} & -c_{\theta_2} + \frac{\lambda_2}{l_s} s_{\theta_2} & c_{\theta_3} + \frac{\lambda_3}{l_s} s_{\theta_3} & -c_{\theta_4} + \frac{\lambda_4}{l_s} s_{\theta_4} \end{bmatrix} \begin{bmatrix} k\omega_1^2 \\ k\omega_2^2 \\ k\omega_3^2 \\ k\omega_4^2 \end{bmatrix}$$

$$M_w = \begin{bmatrix} l_s(F_L^1 - F_L^2 + F_L^3 - F_L^4) \\ l_l(F_L^1 + F_L^2 - F_L^3 - F_L^4) \\ l_s(-F_D^1 + F_D^2 - F_D^3 + F_D^4) \end{bmatrix}$$

and

$$M_{gyro} = \sum_{i=1}^{4} J_{prop} \left[\eta_i \Omega_b \times \begin{bmatrix} c_{\theta_i} \\ 0 \\ -s_{\theta_i} \end{bmatrix} \omega_i \right]$$

In these expressions, l_s and l_l denote the spanwise and longitudinal distances between the rotors and the center of mass of the vehicle, respectively. J_{prop} is the rotational inertia of the rotors about their rotation axes and $\eta_{(1,2,3,4)} = 1, -1, -1, 1$. The rotor reaction torques are modeled as

$$T_i = \lambda_i k \omega_i^2 \tag{13}$$

where λ_i are torque/force ratios. For clockwise rotating propellers, $\lambda_{2,3} = -\lambda$ whereas for counterclockwise rotating propellers $\lambda_{1,4} = \lambda$. In the literature it is reported that λ for such kind of propellers are 0.01–0.05 [23].

Note that the sum of torques created by the rotors result in a roll moment in horizontal flight mode ($\theta_{1,2,3,4} = 0$) and in a yaw moment in vertical flight mode ($\theta_{1,2,3,4} = \pi/2$).

Utilizing vector-matrix notation and including external disturbances, the dynamics of SUAVI can be rewritten in a more compact form as

$$M\dot{\zeta} + C(\zeta)\zeta = G + O(\zeta)\omega + E(\xi)\omega^2 + W(\zeta) + D(\zeta, \xi) \tag{14}$$

where $\zeta = [\dot{X}, \dot{Y}, \dot{Z}, p, q, r]^T$ is the generalized velocity vector and $\xi = [X, Y, Z, \phi, \theta, \psi]^T$ is the position and the orientation (pose) of the vehicle expressed in the world frame. The relation between ζ and ξ is given by the following Jacobian transformation:

$$\dot{\xi} = J\zeta \Rightarrow \begin{bmatrix} \dot{X} \\ \dot{Y} \\ \dot{Z} \\ \dot{\phi} \\ \dot{\theta} \\ \dot{\psi} \end{bmatrix} = \begin{bmatrix} 1 & 0 & 0 & 0 & 0 & 0 \\ 0 & 1 & 0 & 0 & 0 & 0 \\ 0 & 0 & 1 & 0 & 0 & 0 \\ 0 & 0 & 0 & 1 & s_\phi t_\theta & c_\phi t_\theta \\ 0 & 0 & 0 & 0 & c_\phi & -s_\phi \\ 0 & 0 & 0 & 0 & s_\phi / c_\theta & c_\phi / c_\theta \end{bmatrix} \begin{bmatrix} \dot{X} \\ \dot{Y} \\ \dot{Z} \\ p \\ q \\ r \end{bmatrix} \tag{15}$$

Note that the bottom-right 3×3 submatrix of the Jacobian is the inverse of $\mathbb{E}$, i.e. the $\mathbb{B}$ matrix defined in (7).

The mass-inertia matrix M, the Coriolis-centripetal matrix $C(\zeta)$, the gravity term G, and the gyroscopic term $O(\zeta)\omega$, are defined as

$$M = \begin{bmatrix} mI_{3\times3} & 0_{3\times3} \\ 0_{3\times3} & diag(I_{xx}, I_{yy}, I_{zz}) \end{bmatrix} \tag{16}$$

$$C(\zeta) = \begin{bmatrix} 0 & 0 & 0 & 0 & 0 & 0 \\ 0 & 0 & 0 & 0 & 0 & 0 \\ 0 & 0 & 0 & 0 & 0 & 0 \\ 0 & 0 & 0 & 0 & I_{zz} r & -I_{yy} q \\ 0 & 0 & 0 & -I_{zz} r & 0 & I_{xx} p \\ 0 & 0 & 0 & I_{yy} q & -I_{xx} p & 0 \end{bmatrix} \tag{17}$$

$$G = [0, 0, mg, 0, 0, 0]^T \tag{18}$$

$$O(\zeta)\omega = J_{prop} \begin{pmatrix} 0_{3\times1} \\ \sum_{i=1}^{4} [\eta_i \Omega_b \times \begin{bmatrix} c_{\theta_i} \\ 0 \\ -s_{\theta_i} \end{bmatrix} \omega_i] \end{pmatrix} \tag{19}$$

where I_{xx},I_{yy} and I_{zz} are the moments of inertia of the aerial vehicle around its body frame axes.

Lift and drag forces produced by the wings and the resulting moments due to these forces for different wing angles are defined as

$$W(\zeta) = [W_x, W_y, W_z, 0, W_t, 0]^T = \begin{bmatrix} R_{wb} \begin{bmatrix} 2(F_D^f(\theta_f, v_x, v_z) + F_D^r(\theta_r, v_x, v_z)) \\ 0 \\ 2(F_L^f(\theta_f, v_x, v_z) + F_L^r(\theta_r, v_x, v_z)) \\ 0 \end{bmatrix} \\ 2l_l(F_L^f(\theta_f, v_x, v_z) - F_L^r(\theta_r, v_x, v_z)) \\ 0 \end{bmatrix} \quad (20)$$

where $F_L^i(\theta_i, v_x, v_z)$ and $F_D^i(\theta_i, v_x, v_z)$ are the lift and drag forces produced at the wings and $i = f,r$ subscripts denote front and rear angles, respectively. W_x, W_y and W_z are aerodynamic forces along X, Y, Z axis of world coordinate frame and W_t is torques produced by aerodynamic forces around Y axis of body fixed coordinate frame.

System actuator vector, $E(\xi)\omega^2$, is defined as

$$E(\xi)\omega^2 = \begin{bmatrix} R_{wb}F_{th} \\ M_{th} \end{bmatrix} = \begin{bmatrix} (c_\phi s_\theta c_\psi + s_\phi s_\psi)u_v + c_\psi c_\theta u_h \\ (c_\phi s_\theta s_\psi - s_\phi c_\psi)u_v + s_\psi c_\theta u_h \\ c_\phi c_\theta u_v - s_\theta u_h \\ (l_s s_{\theta_f} - \lambda c_{\theta_f})u_{f_{dif}} + (l_s s_{\theta_r} + \lambda c_{\theta_r})u_{r_{dif}} \\ [u_{f_{sum}} s_{\theta_f} - u_{r_{sum}} s_{\theta_r}]l_l \\ (l_s c_{\theta_f} + \lambda s_{\theta_f})u_{f_{dif}} + (l_s c_{\theta_r} - \lambda s_{\theta_r})u_{r_{dif}} \end{bmatrix} \quad (21)$$

where

$$u_{f_{dif}} = k(\omega_1^2 - \omega_2^2), u_{r_{dif}} = k(\omega_3^2 - \omega_4^2), u_{f_{sum}} = k(\omega_1^2 + \omega_2^2),$$
$$u_{r_{sum}} = k(\omega_3^2 + \omega_4^2), u_v = -s_{\theta_f} u_{f_{sum}} - s_{\theta_r} u_{r_{sum}},$$
$$u_h = c_{\theta_f} u_{f_{sum}} + c_{\theta_r} u_{r_{sum}}, \theta_f = \theta_1 = \theta_2, \theta_r = \theta_3 = \theta_4$$

To simplify the analysis, in the sequel the aerodynamic downwash effect of front wings on the rear wings will be neglected and the front and rear wing angles are assumed to be equal ($\theta_f = \theta_r$). In this case the system actuator vector becomes

$$E(\xi)\omega^2 = \begin{bmatrix} (c_\psi c_\theta c_{\theta_f} - (c_\phi s_\theta c_\psi + s_\phi s_\psi)s_{\theta_f})u_1 \\ (s_\psi c_\theta c_{\theta_f} - (c_\phi s_\theta s_\psi - s_\phi c_\psi)s_{\theta_f})u_1 \\ (-s_\theta c_{\theta_f} - c_\phi c_\theta s_{\theta_f})u_1 \\ s_{\theta_f} u_2 - c_{\theta_f} u_4 \\ s_{\theta_f} u_3 \\ c_{\theta_f} u_2 + s_{\theta_f} u_4 \end{bmatrix} \quad (22)$$

Control inputs $u_{1,2,3,4}$ used in (22) are explicitly written below:

$$u_1 = k(\omega_1^2 + \omega_2^2 + \omega_3^2 + \omega_4^2) \quad (23)$$
$$u_2 = kl_s(\omega_1^2 - \omega_2^2 + \omega_3^2 - \omega_4^2) \quad (24)$$
$$u_3 = kl_l(\omega_1^2 + \omega_2^2 - \omega_3^2 - \omega_4^2) \quad (25)$$
$$u_4 = k\lambda(\omega_1^2 - \omega_2^2 - \omega_3^2 + \omega_4^2) \quad (26)$$

Neglecting the wing forces and setting $\theta_f = \theta_r = \pi/2$, the dynamics of the aerial vehicle resembles a quadrotor model reported in the literature [22–24]. Position and attitude dynamics of the aerial vehicle in quadrotor mode can be expressed as follows:

$$\ddot{X} = \frac{1}{m}(-c_\phi s_\theta c_\psi - s_\phi s_\psi)u_1$$
$$\ddot{Y} = \frac{1}{m}(-c_\phi s_\theta s_\psi + s_\phi c_\psi)u_1$$
$$\ddot{Z} = -\frac{c_\phi c_\theta}{m}u_1 + g$$
$$\dot{p} = \frac{u_2}{I_{xx}} + \frac{I_{yy} - I_{zz}}{I_{xx}}qr - \frac{J_{prop}}{I_{xx}}q\omega_p$$
$$\dot{q} = \frac{u_3}{I_{yy}} + \frac{I_{zz} - I_{xx}}{I_{yy}}pr + \frac{J_{prop}}{I_{yy}}p\omega_p$$
$$\dot{r} = \frac{u_4}{I_{zz}} + \frac{I_{xx} - I_{yy}}{I_{zz}}pq \quad (27)$$

where $\omega_p = \omega_1 - \omega_2 - \omega_3 + \omega_4$.

Table 2
Modeling parameters.

Symbol	Description	Magnitude
m	mass	4.5 kg
l_s	Rotor distance to cog along y axis	0.3 m
l_l	Rotor distance to cog along x axis	0.3 m
I_{xx}	Moment of inertia along x axis	0.405 kg m^2
I_{yy}	Moment of inertia along y axis	0.405 kg m^2
I_{zz}	Moment of inertia along z axis	0.72 kg m^2
$\lambda_{1,4}$	Torque/force ratio	0.01 Nm/N
$\lambda_{2,3}$	Torque/force ratio	−0.01 Nm/N

For the transition and the horizontal flight modes, dynamics of the aerial vehicle can be written as

$$\ddot{X} = \frac{1}{m}[(c_\psi c_\theta c_{\theta_f} - (c_\phi s_\theta c_\psi + s_\phi s_\psi)s_{\theta_f})u_1 + W_x]$$
$$\ddot{Y} = \frac{1}{m}[(s_\psi c_\theta c_{\theta_f} - (c_\phi s_\theta s_\psi - s_\phi c_\psi)s_{\theta_f})u_1 + W_y]$$
$$\ddot{Z} = \frac{1}{m}[(-s_\theta c_{\theta_f} - c_\phi c_\theta s_{\theta_f})u_1 + mg + W_z]$$
$$\dot{p} = \frac{u_2}{I_{xx}} + \frac{I_{yy} - I_{zz}}{I_{xx}}qr - \frac{J_{prop}}{I_{xx}}q\omega_p s_{\theta_f}$$
$$\dot{q} = \frac{u_3}{I_{yy}} + \frac{I_{zz} - I_{xx}}{I_{yy}}pr + \frac{J_{prop}}{I_{yy}}(ps_{\theta_f} + rc_{\theta_f})\omega_p + W_t$$
$$\dot{r} = \frac{u_4}{I_{zz}} + \frac{I_{xx} - I_{yy}}{I_{zz}}pq - \frac{J_{prop}}{I_{zz}}q\omega_p c_{\theta_f} \quad (28)$$

Setting the front and rear wing angles to 0°, the dynamical model in transition and horizontal flight modes (28) becomes the model for a four rotor tandem wing airplane as follows:

$$\ddot{X} = \frac{1}{m}[c_\psi c_\theta u_1 + W_x]$$
$$\ddot{Y} = \frac{1}{m}[s_\psi c_\theta u_1 + W_y]$$
$$\ddot{Z} = \frac{1}{m}[-s_\theta u_1 + mg + W_z]$$
$$\dot{p} = \frac{u_2}{I_{xx}} + \frac{I_{yy} - I_{zz}}{I_{xx}}qr$$
$$\dot{q} = \frac{u_3}{I_{yy}} + \frac{I_{zz} - I_{xx}}{I_{yy}}pr + \frac{J_{prop}}{I_{yy}}r\omega_p + W_t$$
$$\dot{r} = \frac{u_4}{I_{zz}} + \frac{I_{xx} - I_{yy}}{I_{zz}}pq - \frac{J_{prop}}{I_{zz}}q\omega_p \quad (29)$$

For the attitude control, the attitude dynamics of the aerial vehicle must be expressed in the world frame. To this end, rotational part of rigid body dynamics given in (8) can be rewritten as

$$\dot{\Omega}_b = I_b^{-1}(-\Omega_b \times (I_b\Omega_b) + M_t) \quad (30)$$

and the derivative of (7) is

$$\dot{\Omega}_w = \dot{\mathbb{B}}\Omega_b + \mathbb{B}\dot{\Omega}_b \quad (31)$$

By using (5) and substituting (30) into (31), the equation becomes

$$\dot{\Omega}_w = \dot{\mathbb{B}}\mathbb{E}\Omega_w - \mathbb{B}I_b^{-1}(\mathbb{E}\Omega_w \times I_b\mathbb{E}\Omega_w) + \mathbb{B}I_b^{-1}M_t \quad (32)$$

Multiplying both sides of (32) by the transformed inertia matrix $\mathbb{M}(\alpha_w) = \mathbb{E}^T I_b \mathbb{E}$ and using the fact that $\dot{\mathbb{E}} = -\mathbb{E}\dot{\mathbb{B}}\mathbb{E}$, the following equation is obtained.

$$\mathbb{M}(\alpha_w)\dot{\Omega}_w = -\mathbb{E}^T I_b \dot{\mathbb{E}}\Omega_w - \mathbb{E}^T(\mathbb{E}\Omega_w \times I_b\mathbb{E}\Omega_w) + \mathbb{E}^T M_t \quad (33)$$

Coriolis terms in above equation can be cast into the matrix $\mathbb{C}$ as

$$\mathbb{C}(\alpha_w, \Omega_w) = +\mathbb{E}^T I_b \dot{\mathbb{E}} - \mathbb{E}^T S(\mathbb{E}\Omega_w) I_b \mathbb{E}$$

Please cite this article in press as: Cetinsoy E et al. Design and construction of a novel quad tilt-wing UAV. Mechatronics (2012), http://dx.doi.org/10.1016/j.mechatronics.2012.03.003

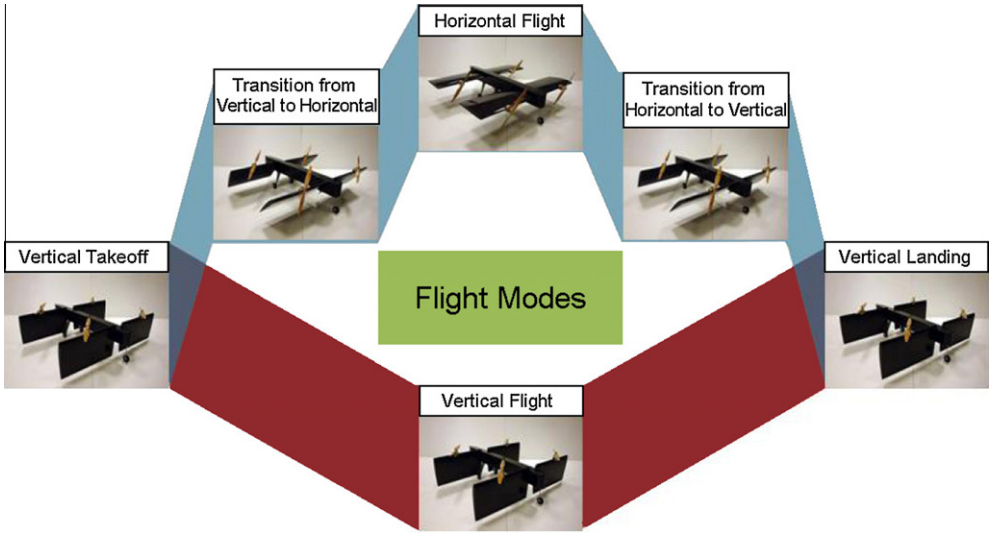

Fig. 18. Two main flight paths of SUAVI.

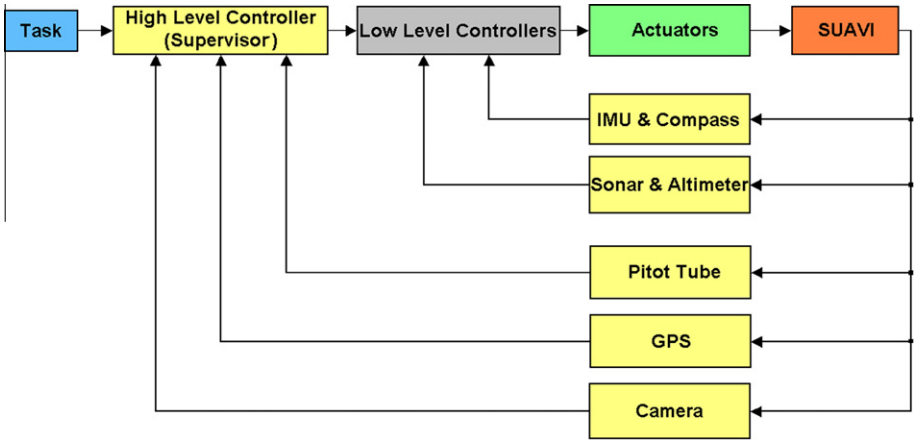

Fig. 19. Hierarchical control architecture.

where $S(.)$ is the skew-symmetric matrix that replaces the cross-product. The attitude dynamics expressed in the world frame can be written in a more compact form as follows

$$\mathbb{M}(\alpha_w)\dot{\Omega}_w + \mathbb{C}(\alpha_w, \Omega_w)\Omega_w = \mathbb{E}^T M_t \tag{34}$$

The parameters of the vehicle used in mathematical modeling are tabulated in Table 2.

3.2. Flight control system

SUAVI has two fundamental flight modes, which are the vertical and horizontal flights (Fig. 18). The wings are vertical during take-off, hovering and landing, and tilted when forward motion is required. The tilt angle is determined based on the requirements of the present flight speed. The control system needs to handle all of these issues for accomplishing the stable flight and successful reference tracking.

To address these issues, a hierarchical control system (Fig. 19) is developed. The high-level controller (supervisor) is responsible for generating feasible trajectories based on GPS and camera data, generating corresponding attitude references for the low-level controllers, switching of the low-level controllers into the closed-loop system depending on the flight mode, forming the communication link with the ground station and performing all checks including security. In case of an emergency such as the lost of the balance of the aircraft in the transition and horizontal flights, this high level control immediately switches the aircraft back into the vertical flight configuration to prevent any crashes. The low-level controllers are responsible for obtaining sensor measurements, performing necessary filtering for reliable state estimations, gathering the human operator inputs on the system and handling the low-level control calculations.

The high-level control is implemented in a Gumstix microcomputer with the GPS, camera and RF communication module being directly connected. The low-level controllers are implemented in microcontroller based control circuit (Fig. 20).

In order to design flight controllers, i.e. position and attitude controllers of vertical, transition and horizontal modes, dynamics of aerial vehicle is divided into two subsystems, namely position and attitude subsystems [25]. Since the position subsystem has slow dynamics, this subsystem is utilized to create reference angles for the attitude subsystem by exploiting the structure of the position subsystem. For simplicity, the downwash effects of the front wings on rear wings will be neglected, therefore equal

Please cite this article in press as: Cetinsoy E et al. Design and construction of a novel quad tilt-wing UAV. Mechatronics (2012), http://dx.doi.org/10.1016/j.mechatronics.2012.03.003

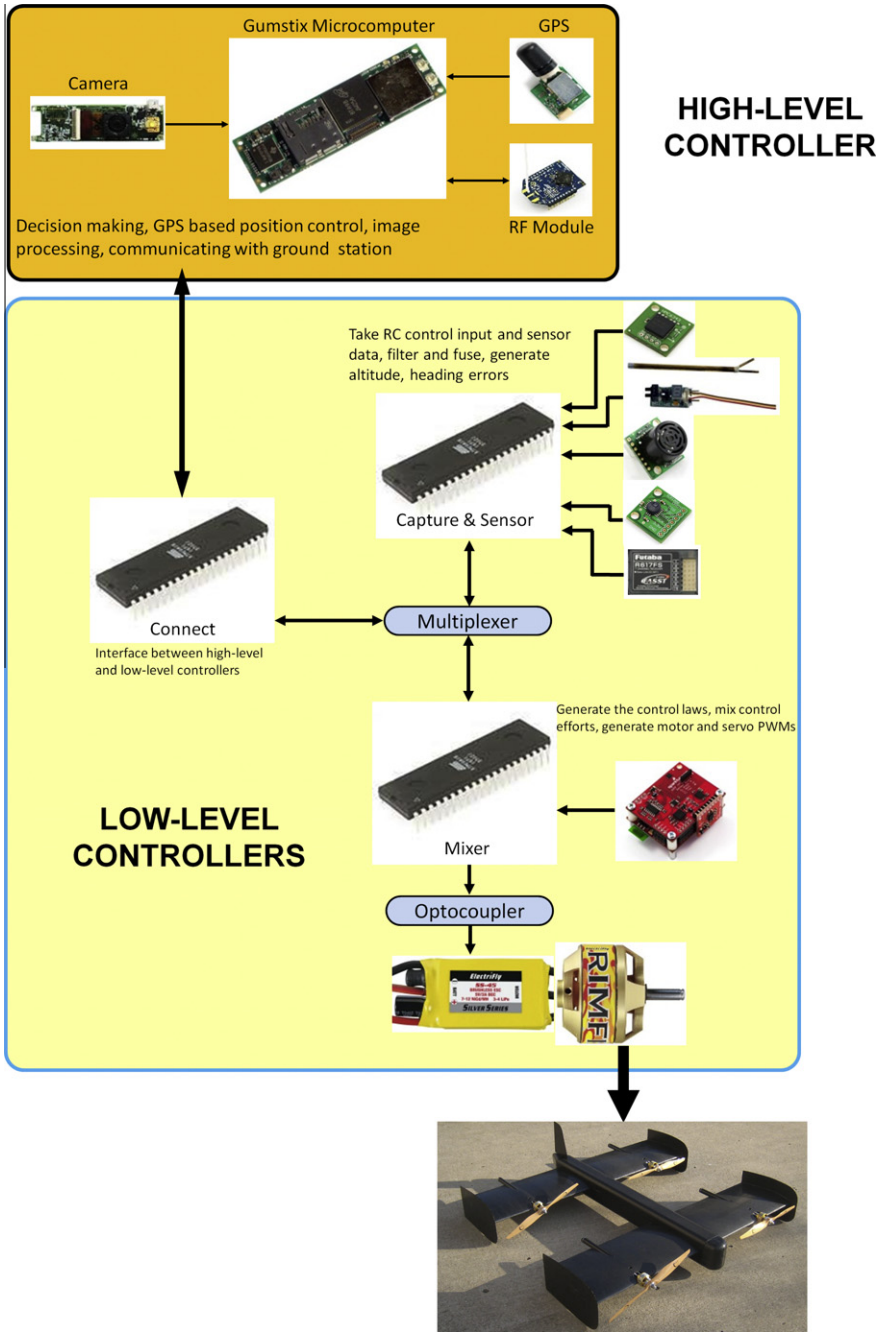

Fig. 20. Flight control system implementation on the hardware.

front and rear wing angles will be assumed, i.e. $\theta_f = \theta_r$. Control calculations will be based on front wing angels. A development without this assumption will be much more involved. However, it should be noted that in practical flight tests a look-up table which is obtained from the wind tunnel tests is used by the high level controller to command the servos to place the rear wings at a higher angle of attack than the front wings.

The roll and pitch references obtained from position controllers presented in Sections 3.2.1, 3.2.2 and 3.2.3 are used in the attitude controllers developed in Section 3.2.4. It should be noted that the same attitude controllers are used in all three flight modes where roll and pitch references are calculated differently depending on the flight mode.

3.2.1. Vertical mode position controllers

In order to design vertical mode position controllers, first the aerial vehicle position (X, Y and Z) dynamics is recalled; i.e.

$$\ddot{X} = \frac{1}{m}[(c_\psi c_\theta c_{\theta_f} - (c_\phi s_\theta c_\psi + s_\phi s_\psi)s_{\theta_f})u_1 + W_x] \tag{35}$$

$$\ddot{Y} = \frac{1}{m}[(s_\psi c_\theta c_{\theta_f} - (c_\phi s_\theta s_\psi - s_\phi c_\psi)s_{\theta_f})u_1 + W_y] \tag{36}$$

$$\ddot{Z} = \frac{1}{m}[(-s_\theta c_{\theta_f} - c_\phi c_\theta s_{\theta_f})u_1 + mg + W_z] \tag{37}$$

The aerial vehicle has to produce required accelerations along X, Y and Z axis, in order to track the desired trajectory in vertical mode.

Please cite this article in press as: Cetinsoy E et al. Design and construction of a novel quad tilt-wing UAV. Mechatronics (2012), http://dx.doi.org/10.1016/j.mechatronics.2012.03.003

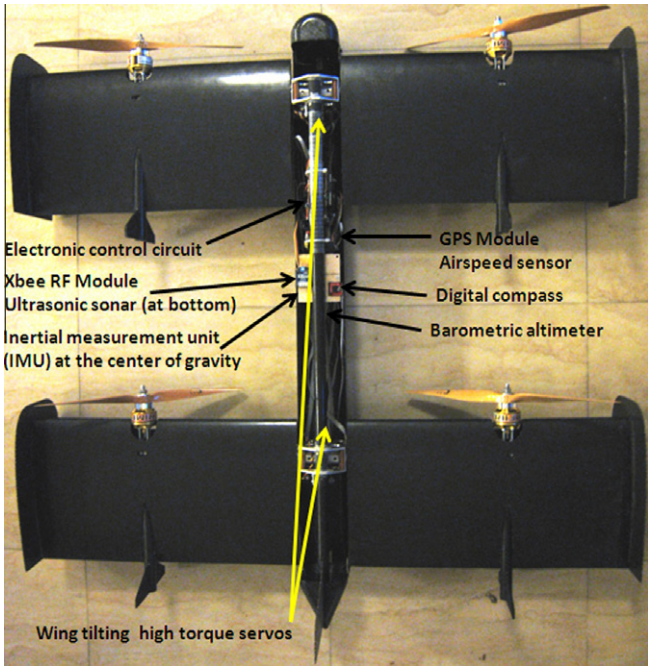

Fig. 21. Electronics mounted on the aerial vehicle.

These accelerations can be generated by virtual control inputs which are designed as PID controllers; i.e.

$$\mu_1 = K_{p_x} e_x + K_{ix} \int_0^t e_x dt + K_{dx} \dot{e}_x \tag{38}$$

$$\mu_2 = K_{p_y} e_y + K_{iy} \int_0^t e_y dt + K_{dy} \dot{e}_y \tag{39}$$

$$\mu_3 = K_{p_z} e_z + K_{iz} \int_0^t e_z dt + K_{dz} \dot{e}_z \tag{40}$$

where position tracking errors are defined as $e_q = q_d - q$ for $q = X, Y, Z$. The aerial vehicle is required to track the desired attitude angles and produce the total thrust to generate the desired acceleration. In order to compute these desired attitude angles and the total thrust, dynamic inversion approach can be utilized. By equating virtual control inputs to position dynamics and transferring gravity and aerodynamic forces to the left hand side of the equation, the following equations are obtained

$$\tilde{\mu}_1 \triangleq m\mu_1 - W_x = (c_{\psi_d} c_{\theta_d} c_{\theta_f} - (c_{\phi_d} s_{\theta_d} c_{\psi_d} + s_{\phi_d} s_{\psi_d}) s_{\theta_f}) u_1 \tag{41}$$

$$\tilde{\mu}_2 \triangleq m\mu_2 - W_y = (s_{\psi_d} c_{\theta_d} c_{\theta_f} - (c_{\phi_d} s_{\theta_d} s_{\psi_d} - s_{\phi_d} c_{\psi_d}) s_{\theta_f}) u_1 \tag{42}$$

$$\tilde{\mu}_3 \triangleq m\mu_3 - W_z - mg = (-s_{\theta_d} c_{\theta_f} - c_{\phi_d} c_{\theta_d} s_{\theta_f}) u_1 \tag{43}$$

where $\tilde{\mu}_1, \tilde{\mu}_2$ and $\tilde{\mu}_3$ are new virtual inputs. Eqs. (41)–(43) can be solved for the total thrust u_1, desired roll (ϕ_d) and pitch (θ_d) angles as

$$u_1 = \sqrt{\tilde{\mu}_1^2 + \tilde{\mu}_2^2 + \tilde{\mu}_3^2} \tag{44}$$

$$\phi_d = \arcsin\left(\frac{\gamma_2}{u_1 \cdot s_{\theta_f}}\right) \tag{45}$$

$$\theta_d = \arcsin\left(\frac{-\tilde{\mu}_3 \cdot u_1 \cdot c_{\theta_f} - u_1 \cdot \gamma_1 \cdot s_{\theta_f} \cdot c_{\phi_d}}{\gamma_1^2 + \tilde{\mu}_3^2}\right) \tag{46}$$

where γ_1 and γ_2 are the auxiliary variables and they are defined as

$$\gamma_1 = \tilde{\mu}_1 \cdot c_{\psi_d} + \tilde{\mu}_2 \cdot s_{\psi_d} \tag{47}$$

$$\gamma_2 = \tilde{\mu}_1 \cdot s_{\psi_d} - \tilde{\mu}_2 \cdot c_{\psi_d} \tag{48}$$

Desired roll and pitch angles computed using (45) and (46) will be references for the attitude subsystem. It should be noted that the desired yaw angle can be set to any reference value. Note that the total thrust and the desired attitude angles are functions of the wing angles ($\theta_f = \theta_r$). In the literature there exists such reference angle calculations for quadrotors [25], however calculations that depend on wing angles are not studied for tilt-wing or tilt-rotor quadrotors. Our developments here provide reference angles for quadrotors that have tilted wings or rotors.

Remark 1. SUAVI behaves like a quadrotor when the wing angles are set to an angle higher than 70° (tilted 20° from the vertical). To see this, recall that $\sin(70) \approx 0.94$ and therefore the vertical thrust component dominates the horizontal one.

3.2.2. Transition mode position controllers

These position controllers are employed during the transition between the vertical ($\theta_f = \theta_r = 90°$) and the horizontal ($\theta_f = \theta_r < 30°$) wing angles. Since wings are tilted in this flight mode, forward (X axis direction) acceleration of the aerial vehicle is produced by horizontal component of the total thrust. The purpose of transition mode position controllers is to keep the altitude of the aerial vehicle at some desired value. By setting $\tilde{\mu}_1 = 0$, the total thrust and the desired roll angle for this flight mode can be computed as

$$u_1 = \sqrt{\tilde{\mu}_2^2 + \tilde{\mu}_3^2} \tag{49}$$

$$\phi_d = \arcsin\left(\frac{-\tilde{\mu}_2 \cdot c_{\psi_d}}{u_1 \cdot s_{\theta_f}}\right) \tag{50}$$

Virtual inputs $\tilde{\mu}_2$ and $\tilde{\mu}_3$ that appear in above equations can be computed by utilizing controllers given in (39) and (40) and (42) and (43). Calculated desired roll angle is a reference angle for attitude subsystem and it is required to direct motor thrusts. The desired pitch angle is set to zero ($\theta_d = 0$) in order to make the fuselage parallel to the ground and the desired yaw angle is set arbitrarily in transition mode.

Rolling and pitching moments are handled by the attitude controllers presented in Section 3.2.4 since attitude controllers are common in all three flight modes. Desired roll angle calculated by (50) and the desired pitch angle ($\theta_d = 0$) are utilized as references in the computation of virtual control inputs designed as PID controllers given in (59)–(61). In light of feedback linearizing virtual controller given in (54), rolling and pitching moments can be computed using (62) and (63). Since the attitude controllers are designed as robust feedback linearizing controllers, desired rolling and pitching moments are properly generated to prevent the UAV from crashing.

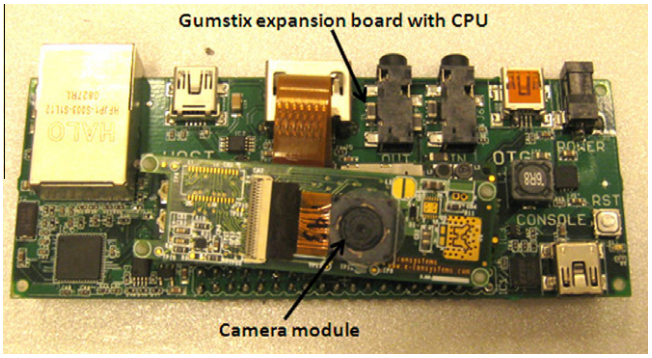

Fig. 22. Gumstix Overo microcomputer with its onboard camera.

Please cite this article in press as: Cetinsoy E et al. Design and construction of a novel quad tilt-wing UAV. Mechatronics (2012), http://dx.doi.org/10.1016/j.mechatronics.2012.03.003

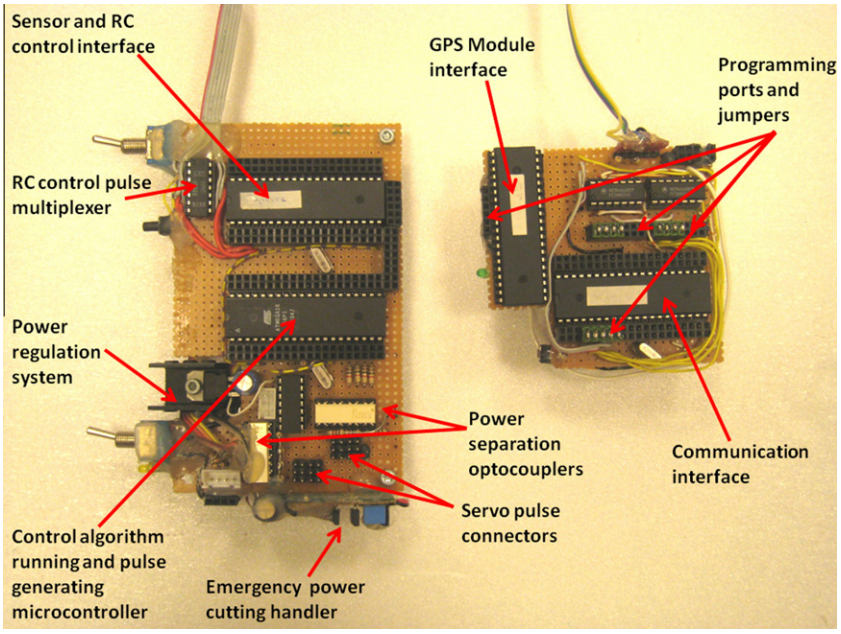

Fig. 23. Low-level control circuit.

3.2.3. Horizontal mode position controllers

After the wings are tilted to the desired angle, horizontal control is activated. In this flight mode acceleration along Z direction is produced by vertical component of the total thrust which is created by tilted wings. The purpose of the horizontal flight mode is to track given trajectory along X and Y axes. For the trajectory tracking along X axis the total thrust will be used. For the tracking along Y axis the vertical component of the total thrust is directed by rolling the aerial vehicle. In order to design the controller for X axis and compute the total thrust, dynamics of X can be linearized as

$$\ddot{X} = \frac{1}{m}(u_1 c_{\theta_f} + W_x) \tag{51}$$

The following PID controller is designed for the linearized dynamics:

$$u_1 = K_{p_x} e_x + K_{ix} \int_0^t e_x dt + K_{dx} \dot{e}_x - \frac{W_x}{c_{\theta_f}} \tag{52}$$

where position tracking error is defined as $e_x = X_d - X$. As in vertical mode, the total thrust is directed by rolling the aerial vehicle. Desired roll angle can again be computed using (50). But in this case, the total thrust u_1 is calculated from (52). Similar to the transition mode, desired roll angle is a reference angle for attitude subsystem and desired pitch angle is set to zero ($\theta_d = 0$) in order to make the fuselage parallel to the ground. Yaw angle reference is given arbitrarily in horizontal mode.

3.2.4. Attitude controllers

Attitude controllers are the same for all three flight modes. Desired attitude angles given in Sections 3.2.1, 3.2.2 and 3.2.3 position controller section are used as reference angles. To design attitude controllers, (34) can be rewritten as

$$\mathbb{M}(\alpha_w)\dot{\Omega}_w + \mathbb{C}(\alpha_w, \Omega_w)\Omega_w = \mathbb{E}^T(M_{th} + M_w) \tag{53}$$

where $M_t \approx M_{th} + M_w$. Note that gyroscopic effects included in M_t are neglected. Since gyroscopic effects on propellers are small enough to be neglected, these moments are not considered in controller design. The attitude dynamics given in (53) is fully actuated, therefore it is feedback linearizable. Consider the following transformation for feedback linearization:

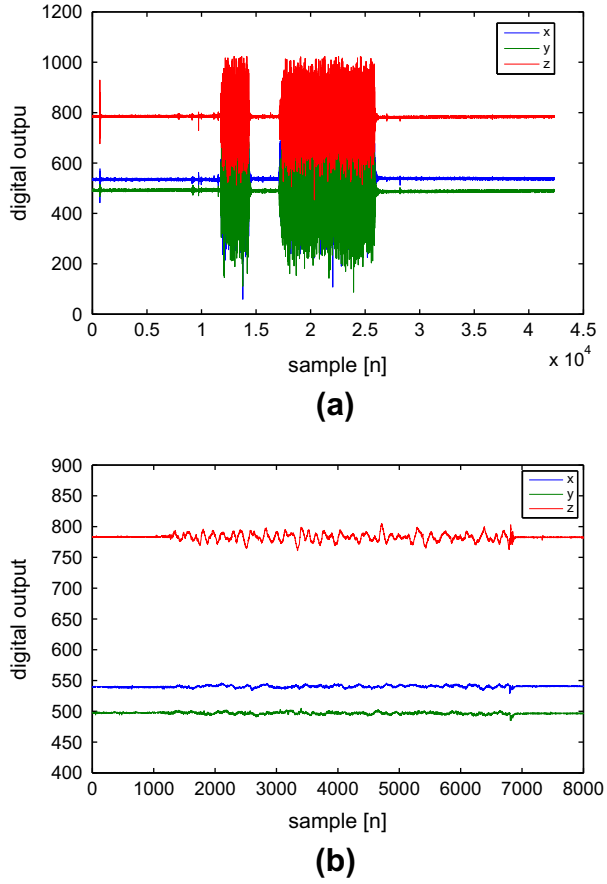

Fig. 24. Accelerometer readings around x, y, z axes during hover without (a) and with anti-aliasing filters.

Please cite this article in press as: Cetinsoy E et al. Design and construction of a novel quad tilt-wing UAV. Mechatronics (2012), http://dx.doi.org/10.1016/j.mechatronics.2012.03.003

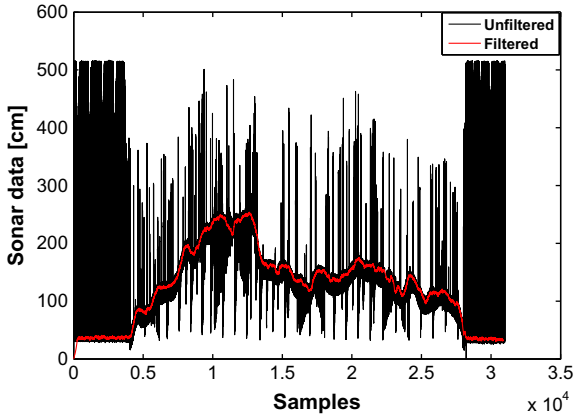

Fig. 25. The raw and the filtered altitude measurements from sonar.

$$\tilde{\eta} = M_{th} = I_b \mathbb{E}\eta + \mathbb{E}^{-T}\mathbb{C}(\alpha_w, \Omega_w)\Omega_w - M_w \tag{54}$$

where $\tilde{\eta}$ is a new virtual control input vector and η is the virtual control input vector for attitude subsystem. These control inputs have three components and they are defined as

$$\tilde{\eta} = [\,\tilde{\eta}_4 \quad \tilde{\eta}_5 \quad \tilde{\eta}_6\,]^T, \eta = [\,\eta_4 \quad \eta_5 \quad \eta_6\,]^T \tag{55}$$

In light of (22), (54) and (55), it follows that

$$\tilde{\eta}_4 = s_{\theta_f} u_2 - c_{\theta_f} u_4 \tag{56}$$

$$\tilde{\eta}_5 = s_{\theta_f} u_3 \tag{57}$$

$$\tilde{\eta}_6 = c_{\theta_f} u_2 + s_{\theta_f} u_4 \tag{58}$$

The following PID controllers are designed to generate virtual control inputs, η_4,η_5,η_6; i.e.

$$\eta_4 = K_{p_\phi} e_\phi + K_{i_\phi} \int_0^t e_\phi dt + K_{d_\phi} \dot{e}_\phi \tag{59}$$

$$\eta_5 = K_{p_\theta} e_\theta + K_{i_\theta} \int_0^t e_\theta dt + K_{d_\theta} \dot{e}_\theta \tag{60}$$

$$\eta_6 = K_{p_\psi} e_\psi + K_{i_\psi} \int_0^t e_\psi dt + K_{d_\psi} \dot{e}_\psi \tag{61}$$

where attitude tracking errors are defined as $e_q = q_d - q$ for $q = \phi, \theta, \psi$. It should again be emphasized that in vertical flight mode desired roll and pitch angles (ϕ_d, θ_d) are computed from position subsystem, whereas in transition and horizontal flight mode only desired roll angle is computed from position subsystem. Pitch angle reference for transition and horizontal mode is set to $\theta_d = 0$. On the other hand, the desired yaw angle is specified by the user or the high level controller for all three flight modes.

It is well known that physical inputs for quadrotor type aerial vehicles are rotor rotational speeds that generate motor thrusts. The relationship between control inputs and rotor speeds is given through (23)–(26) The total thrust u_1 generated by rotors is given in (44), (49) and (52) for vertical, transition and horizontal modes, respectively. In light of (56)–(58), the other control inputs u_{2-4} can easily be found as

$$u_3 = \frac{\tilde{\eta}_5}{s_{\theta_f}} \tag{62}$$

$$\begin{bmatrix} u_2 \\ u_4 \end{bmatrix} = \begin{bmatrix} s_{\theta_f} & -c_{\theta_f} \\ c_{\theta_f} & s_{\theta_f} \end{bmatrix}^{-1} \begin{bmatrix} \tilde{\eta}_4 \\ \tilde{\eta}_6 \end{bmatrix} \tag{63}$$

4. Control system hardware

The electronic flight control system of SUAVI utilizes various sensors for situational awareness, actuators to apply the required control efforts on the plant and several filters to make the sensor data more accurate and reliable. The prototype with all the electronics mounted is shown in Fig. 21.

The high-level controller in the hierarchical control system of SUAVI is implemented in a *Gumstix*® microcomputer (Fig. 22). As the high-level controller, Gumstix utilizes data from the GPS and the camera that is connected to the camera port of OMAP3530 processor. The image processing based operations are performed using the OpenCV library. The DSP core on the microcomputer allows the computations of image processing algorithms at higher speeds due to its high computational power.

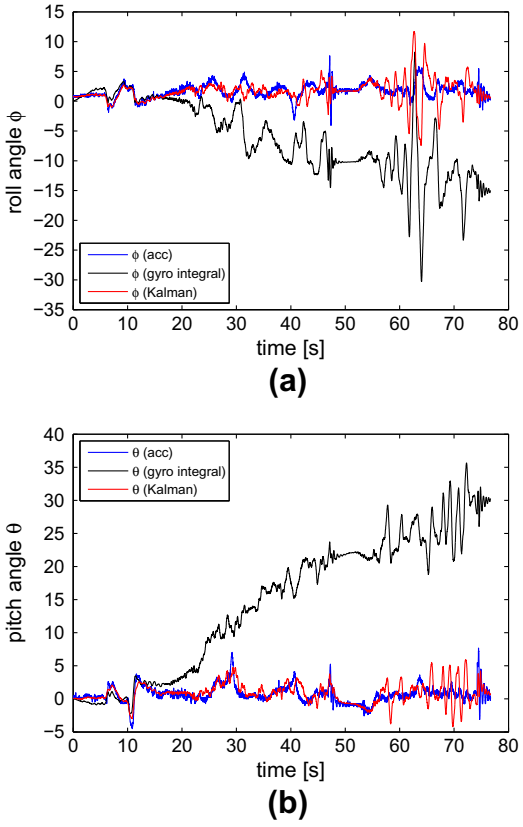

Fig. 26. Kalman filter results in roll (a) and pitch (b) during flight.

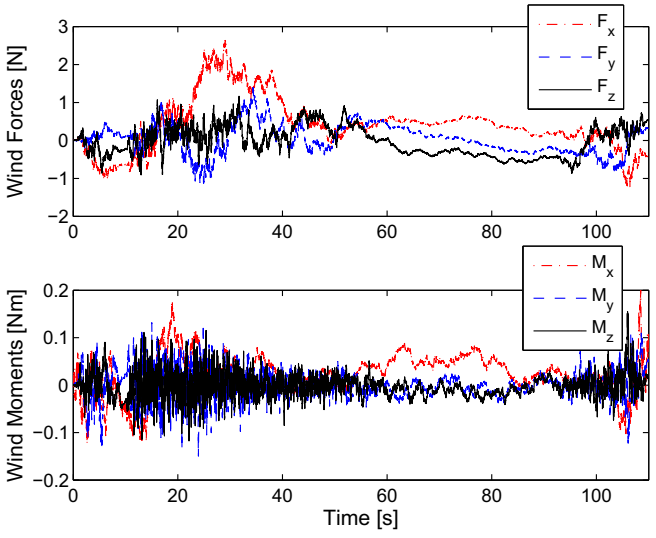

Fig. 27. Wind forces and moments.

Please cite this article in press as: Cetinsoy E et al. Design and construction of a novel quad tilt-wing UAV. Mechatronics (2012), http://dx.doi.org/10.1016/j.mechatronics.2012.03.003

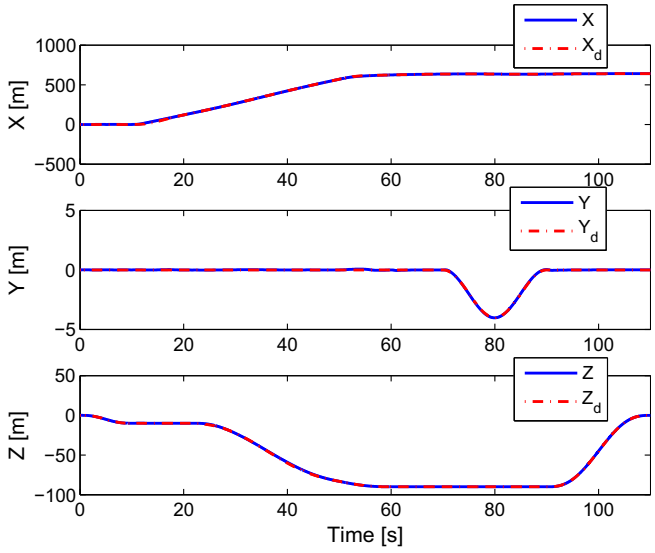

Fig. 28. Position tracking performance.

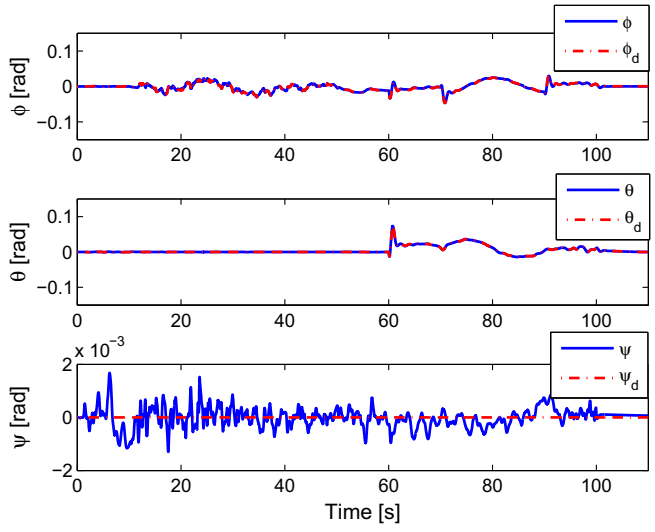

Fig. 29. Attitude tracking performance.

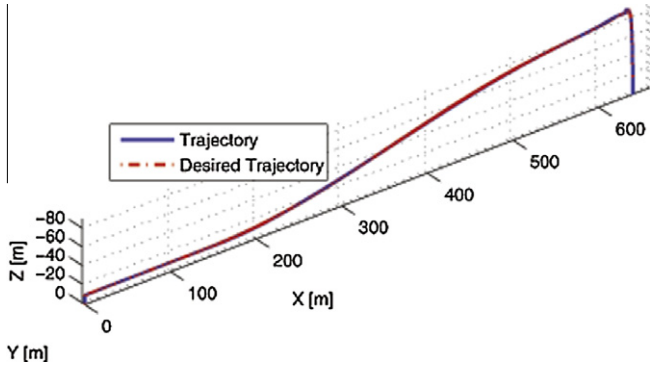

Fig. 30. Trajectory tracking.

The low-level control circuit that is realized for SUAVI is based on three Atmel Atmega16 microcontrollers (Fig. 23). These microcontrollers are given separate tasks that are hard real-time, soft

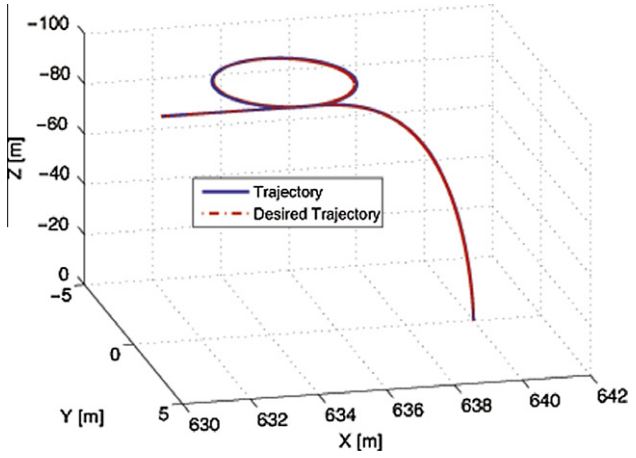

Fig. 31. Trajectory tracking and landing in the vertical mode.

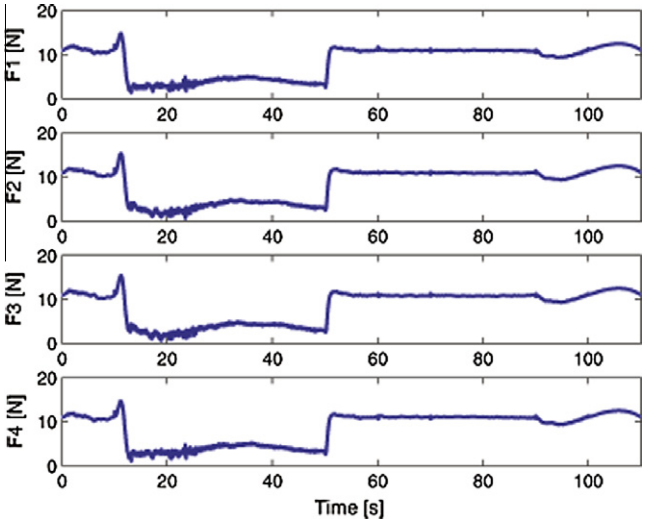

Fig. 32. Motor thrusts.

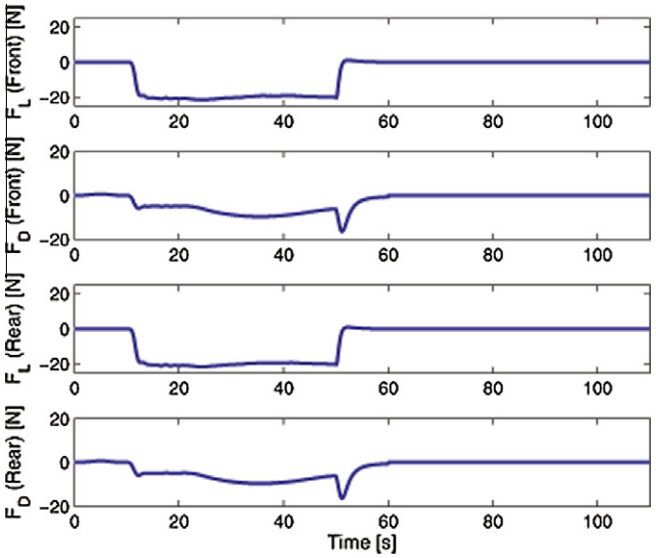

Fig. 33. Aerodynamic forces.

Please cite this article in press as: Cetinsoy E et al. Design and construction of a novel quad tilt-wing UAV. Mechatronics (2012), http://dx.doi.org/10.1016/j.mechatronics.2012.03.003

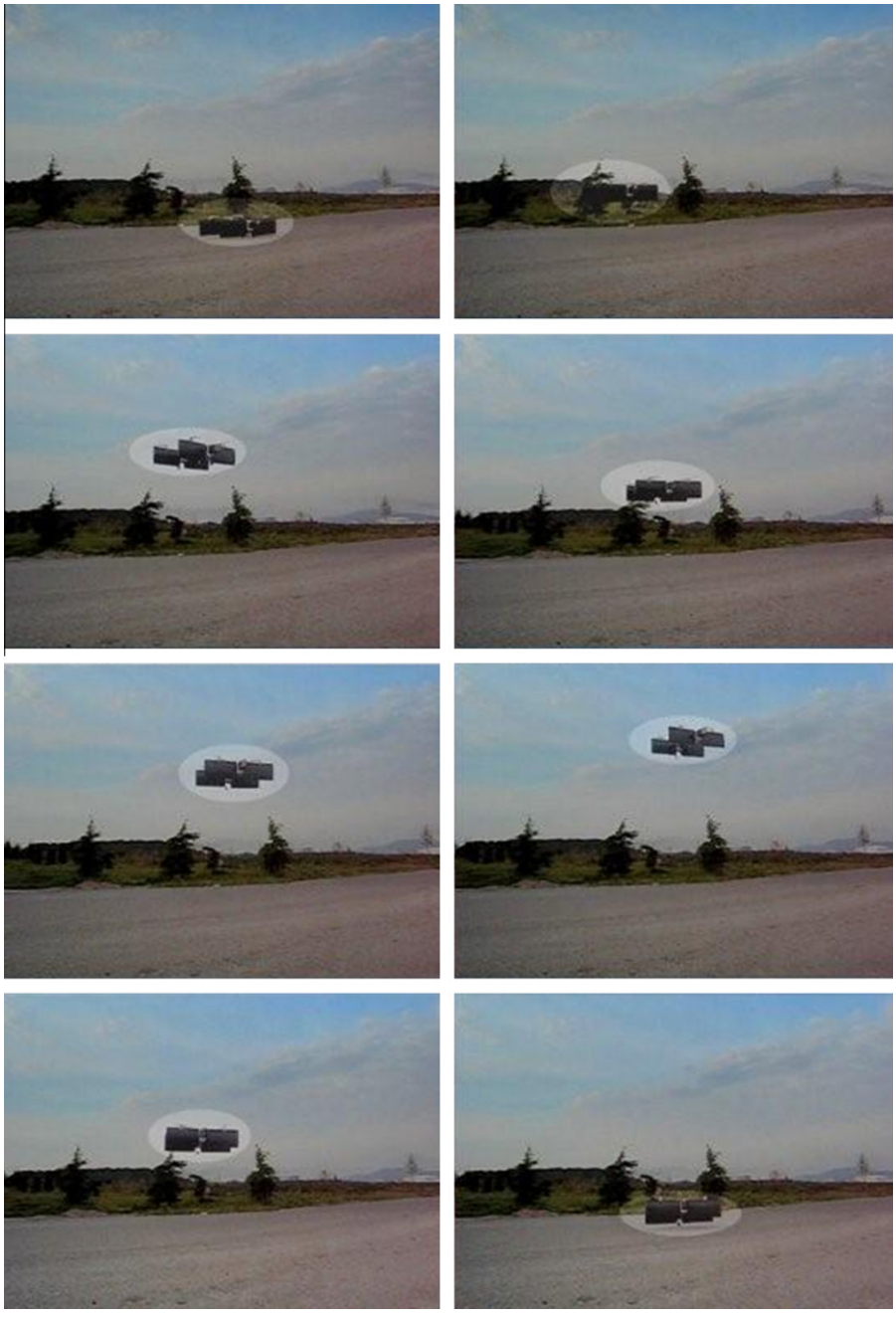

Fig. 34. Outdoor hover test with SUAVI in university campus.

real-time or sporadic tasks. This separation guarantees the operation of the 100 Hz hard real-time control loop without missing any deadline.

4.1. Sensors

To achieve satisfactory stabilization and trajectory tracking tasks, reliable state estimates need to be acquired by the hierarchical control system. For obtaining these reliable state estimates, various sensors are utilized in SUAVI. A Sparkfun 6 DOF v4 inertial measurement unit (IMU) is utilized for the estimation of roll, pitch, yaw angles and angular velocities through its 3-axis accelerometer, 3-axis gyro, 3-axis magnetometer. It is placed on the aerial vehicle's center of mass to obtain more accurate attitude information. A Honeywell HMC6343 tilt-compensated magnetometer is included in the system for reliable heading measurements. For above the ground altitude measurement, a Maxbotix EZ4 sonar with 2.54 cm (1″) of resolution for up to 6.45 m distance is used.

A VTI Technologies SCP1000 altimeter with 10 cm resolution is utilized for above the sea level altitude measurements at higher altitudes and an Eagle Tree Airspeed MicroSensor V3 airspeed sensor with pitot tube is used for the horizontal airspeed measurements. An ADH Technology D2523T GPS unit with a high-gain active antenna and 50 channel GPS receiver circuits, which can deliver 2 Hz GPS data is embedded in the system for world coordinate estimations.

4.2. Actuators

To apply the forces demanded by the control system for the stable flight of SUAVI in all possible flight conditions, reliable and highly capable actuators are required. Great Planes Rimfire

Please cite this article in press as: Cetinsoy E et al. Design and construction of a novel quad tilt-wing UAV. Mechatronics (2012), http://dx.doi.org/10.1016/j.mechatronics.2012.03.003

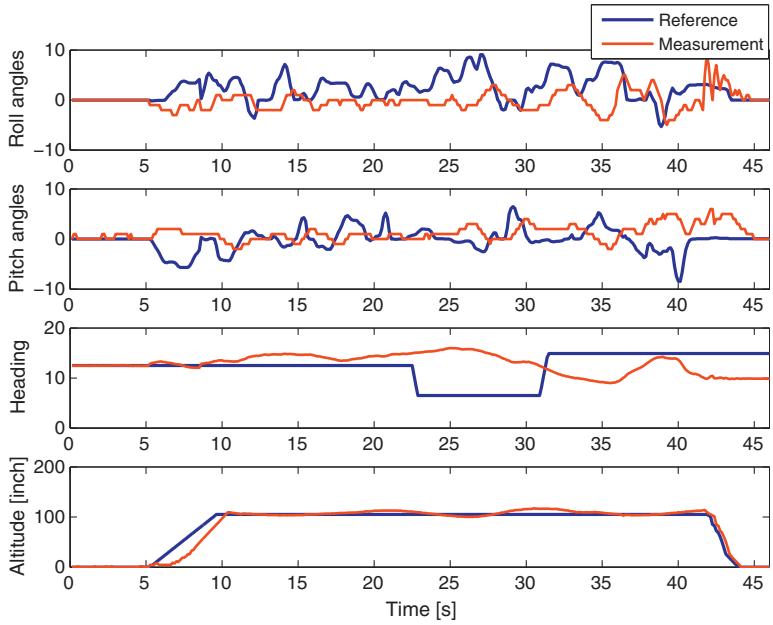

Fig. 35. Vertical flight data of SUAVI.

42-40-800 is chosen among a variety of RC aircraft electric motors for propulsion, since it is a high efficiency direct drive brushless motor. It can deliver more than 1.6 kg of thrust with 14 × 7 in. propellers. For controlling the motor speeds, Great Planes Electrifly Silver Series 35 motor driver is preferred, which is capable of delivering up to 35 A continuously, where the maximum allowed current of the chosen motor is 32 A.

For tilting the wings in the horizontal-vertical range, TS170 high torque digital RC servos with 18 kg cm torque and titanium gears are utilized. They are deliberately chosen that way to ensure very robust wing orientation even in the existence of disturbances of wind gusts and also during landing.

4.3. Filters

In order to obtain reliable feedback signals for flight control system, several analog and digital filters are implemented in the control system of SUAVI.

4.3.1. Analog anti-aliasing filter

The vibrations that are mainly induced by the rotating propellers cause severe noise on the accelerometer readings (Fig. 24a). Analog anti-aliasing filters with 0.6 Hz cut-off frequency are applied on the analog outputs of the accelerometers to cope with it. The inclusion of this low-pass filter brings reasonable readings for the utilization in the sensor fusion (Fig. 24b).

4.3.2. Digital exponentially weighted moving average filter

The noisy sonar reading (Fig. 25) for the distance between the aircraft and the ground is handled by a digital exponentially weighted moving average filter. This filter gives an estimation of the height, which is a convex combination of the filter output in the previous step and the current raw sensor measurement where the coefficient of the raw sensor measurement α is calculated adaptively as:

$$\alpha = \frac{|\Delta S|}{|\Delta S|^{\delta_1} + (|\Delta S|^{\delta_2} + \varepsilon)^{-1}} \tag{64}$$

where $\Delta S = S_t - S_{t-1}$, S_t is the raw measurement at time t, $\delta_1 = 1.4$, $\delta_2 = 0.2$ and $\varepsilon = 0.1$.

4.3.3. Sensor fusion via Kalman filter

To obtain accurate roll and pitch estimations, an Extended Kalman Filter (EKF) algorithm is implemented. Gyros in the IMU have reliable angular rate measurements, however it is not possible to estimate angular position through integrating the gyro readings, since due to integration even a small offset grows without any bound (Fig. 26). Accelerometer based orientation estimation does not suffer from this drift, but it is delayed due to the anti-aliasing filters applied for filtering the noise. EKF is utilized for combining the fast response and no drift advantages of these two sensors to get a reliable attitude estimation [26,27]. We should emphasize the fact that this Euler angle estimation method is only valid for the case of non-maneuvering flight conditions.

In EKF, the state transition (propagation) and observation (measurement) models are nonlinear functions of state and inputs. Therefore, the following non-linear dynamic model is used as a system model for the design of the filter.

$$x_k = f(x_{k-1}, u_{k-1}) + \eta_{k-1} \tag{65}$$

$$z_k = h(x_k) + v_k \tag{66}$$

where η_k and v_k are process and measurement noises with covariance matrices Q and R, respectively. In light of (7), it follows that

$$\dot{\alpha}_w = \Omega_w = \mathbb{B}(\phi, \theta) \cdot \Omega_b \tag{67}$$

or,

$$\begin{bmatrix} \dot{\phi} \\ \dot{\theta} \\ \dot{\psi} \end{bmatrix} = \begin{bmatrix} 1 & s_\phi t_\theta & c_\phi t_\theta \\ 0 & c_\phi & -s_\phi \\ 0 & s_\phi / c_\theta & c_\phi / c_\theta \end{bmatrix} \begin{bmatrix} p \\ q \\ r \end{bmatrix} \tag{68}$$

Discretizing (68) using approximate derivative, we obtain

$$\alpha_{w_k} = \alpha_{w_{k-1}} + T\mathbb{B}(\alpha_{w_{k-1}})\Omega_{b_{k-1}} \tag{69}$$

State evolution will then be governed by

$$x_k \triangleq \begin{bmatrix} \alpha_w \\ b_g \end{bmatrix}_k = \begin{bmatrix} \alpha_{w_{k-1}} + T\mathbb{B}(\alpha_{w_{k-1}})\Omega_{b_{k-1}} \\ b_{g_{k-1}} + \eta_{g_{k-1}} \end{bmatrix} \tag{70}$$

where $b_g \in \mathbb{R}^3$ denotes the bias in gyros, T refers to the sampling time and η_g is the noise associated with the gyro bias. Kalman filter corrects the bias term at each cycle by comparing the estimation of

Please cite this article in press as: Cetinsoy E et al. Design and construction of a novel quad tilt-wing UAV. Mechatronics (2012), http://dx.doi.org/10.1016/j.mechatronics.2012.03.003

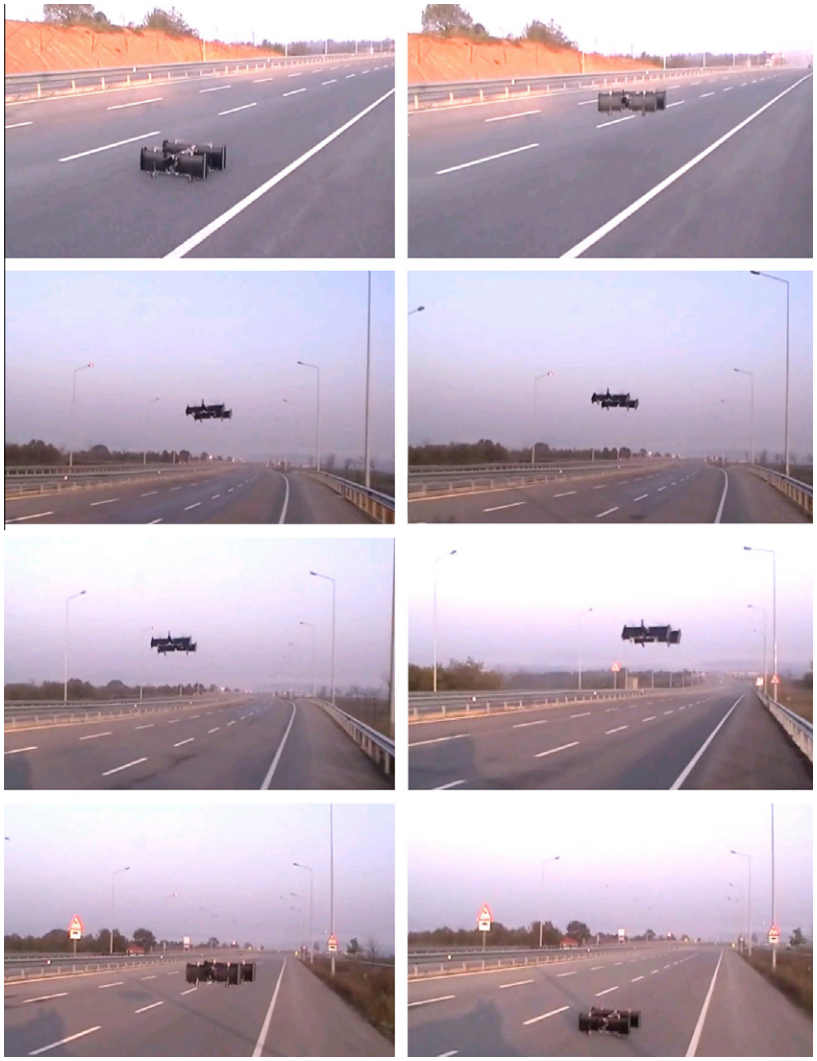

Fig. 36. Horizontal flight snapshots of SUAVI.

angle with the measurements coming from the accelerometers. The filter has two steps: prediction and correction. Prediction equations are:

$$\hat{x}_{k|k-1} = f(\hat{x}_{k-1|k-1}, u_{k-1}) \tag{71}$$

and

$$P_{k|k-1} = A_{k-1}P_{k-1|k-1}A_{k-1}^T + Q_{k-1} \tag{72}$$

Correction equations are:

$$K_k = P_{k|k-1}H_k^T\left(H_kP_{k|k-1}H_k^T + R_k\right)^{-1} \tag{73}$$

$$\hat{x}_{k|k} = \hat{x}_{k|k-1} + K_k(z_k - H\hat{x}_{k|k-1}) \tag{74}$$

and

$$P_{k|k} = (I - K_kH_k)P_{k|k-1} \tag{75}$$

where A and H matrices are defined as

$$A_{k-1} = \left.\frac{\partial f}{\partial x}\right|_{\hat{x}_{k-1,k-1},u_{k-1}} \tag{76}$$

$$H_k = [I_{2\times2} \quad 0_{2\times4}] \tag{77}$$

The nonlinear mapping $h(x_k)$ that defines the accelerometer outputs in terms of Euler angles is quite involved. Instead of working with such a complicated mapping, the measurement matrix (H) is simply formed by concatenating a 2×2 identity matrix with a 2×4 zero matrix to indicate that roll and pitch angles can be obtained from the measurements of the accelerometers using simple trigonometric relations. $P_{k|k-1}$ in (72) is known as a priori error covariance matrix and is used in (73) to compute Kalman gain (K_k). The optimal state vector $\hat{x}_{k|k}$ is calculated as the sum of predicted state vector $\hat{x}_{k|k-1}$ and the correction term $K_k(z_k - H\hat{x}_{k|k-1})$ which is computed by measurements coming from the accelerometers. $P_{k|k}$ in (75) refers to posteriori error covariance matrix and is used to update $P_{k|k-1}$ in (72). Note that the filter needs initial conditions of $\hat{x}_0$ and $P_{0|0}$.

The elements of Q and R matrices in Kalman filter can be tuned experimentally. This may enhance the performance of the filter. In our work, they are selected as follows:

$$Q = \begin{bmatrix} 0.0001 & 0 \\ 0 & 0.000001 \end{bmatrix}, R = \begin{bmatrix} 0.2 & 0 \\ 0 & 0.2 \end{bmatrix} \tag{78}$$

Please cite this article in press as: Cetinsoy E et al. Design and construction of a novel quad tilt-wing UAV. Mechatronics (2012), http://dx.doi.org/10.1016/j.mechatronics.2012.03.003

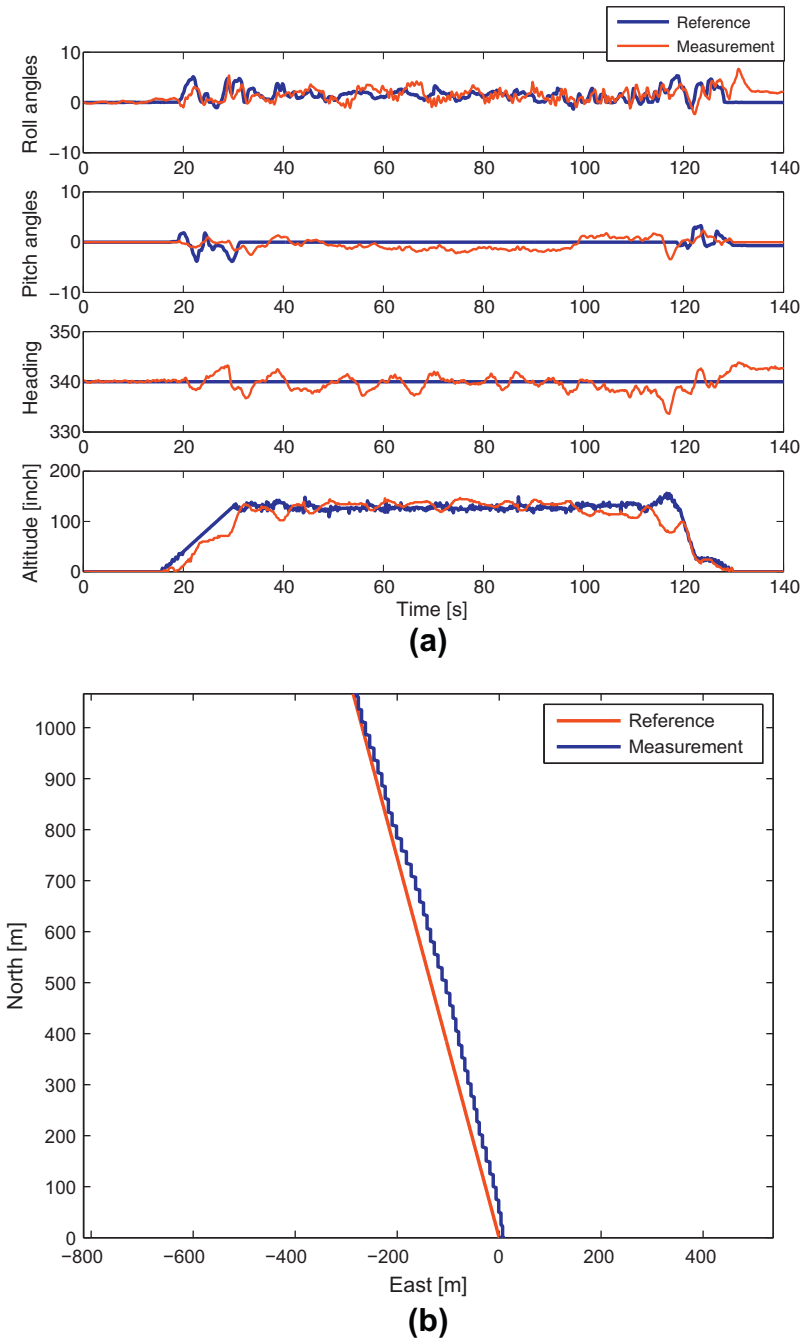

Fig. 37. Horizontal flight attitude, altitude (a) and GPS position (b) data of SUAVI.

EKF is implemented in the onboard microprocessors of the vehicle. The correct estimation of the roll and pitch angles are achieved and the drifts are eliminated. In a real flight experiment where the vertical flight and hover are realized, it is observed that EKF corrects the bias term periodically and delivers driftless roll and pitch estimations (Fig. 26). Since the aircraft is designed for surveillance missions, it is desired to have stable flight with relatively low roll and pitch angles. This is why the roll/pitch movements are small in Fig. 26.

5. Simulation and experimental results

Performance of the proposed controllers on the aerial vehicle are first evaluated in several simulations and then tested in real flight experiments.

5.1. Simulation results

The simulations are carried out in Matlab/Simulink environment. A typical surveillance scenario is considered where during the first 10 sec, the aerial vehicle takes off and climbs to 10 m in vertical mode ($\theta_f = \theta_r = 90°$). Then it begins to tilt its wings between 10 and 0 sec, while it is moving in X direction and preserving its altitude. After wings reach 17° angle of attack in transition mode, the aerial vehicle flies to the desired location in horizontal mode with constant 17° wing angle between 20 and 50 sec. Then, the aerial vehicle tilts its wings back to 90° in transition mode (50–60 sec) and then tracks a circular trajectory in vertical mode (60–90 sec). Finally it lands in 20 sec in vertical mode. Throughout the flight, desired yaw is set to 0°. In order to test performance of the developed controllers, external disturbances are also

Please cite this article in press as: Cetinsoy E et al. Design and construction of a novel quad tilt-wing UAV. Mechatronics (2012), http://dx.doi.org/10.1016/j.mechatronics.2012.03.003

included. These external disturbances are generated as forces and moments produced by wind that is modeled using Dryden Wind-Gust model [28] and depicted in Fig. 27.

Position and attitude tracking performance are depicted in Figs. 28 and 29, respectively. Note that altitudes take negative values, since the Z axis in the world frame is directed downwards. As can be seen from the figures, the aerial vehicle successfully tracks the desired trajectory. During transition and horizontal flight (10–60 sec), pitch angle is set to 0° and roll angle is changing frequently to counteract wind forces and moments. On the other hand, the aerial vehicle continuously changes its attitude to track desired trajectory in vertical mode (60–110 sec).

Fig. 30 demonstrates trajectory tracking performance throughout the flight and Fig. 31 shows trajectory tracking and landing performance in vertical mode. After successful horizontal flight the aerial vehicle tracks circular trajectory and lands on the desired position ([640, 0, 0]) in vertical mode.

Fig. 32 depicts motor thrusts produced by rotors. Notice that in vertical mode, each motor produces approximately 11.25 N to compensate the aerial vehicle's weight. Due to tilted motors and wings, vertical component of the total thrust decreases in transition mode (10–20 and 50–60 sec). Hence, in order to counteract aerial vehicle's weight higher motor thrusts are needed. As can be seen from the figure motor thrusts increase without exceeding maximum capacity of motors, 16 N, in transition mode. On the other hand, motor thrusts are reduced to their 20% due to the lift forces (Fig. 33) generated by wings in horizontal mode (20–50 sec). Since the aerial vehicle consumes less power and saves energy, the flight endurance increases and the vehicle flies longer with the same battery capacity.

5.2. Flight test results

The prototype is also tested for flight with the developed control system. First, vertical flight tests are performed in several areas of Sabanci University campus and on a wide road outside the campus under average wind and gust conditions. Fig. 34 depicts a vertical flight test of the prototype where the attitude and the altitude flight data are depicted in Fig. 35. Despite the existence of large vertical surfaces (wings) in the vertical flight mode, the flight of the aircraft is found to be stable and promising. The roll, pitch and heading angles did not exceed the reference angles for more than 10° during the flight and the deviation of the altitude was bounded by a total of 30 cm. The aircraft is drifted by the winds due to its vertical wings, which act like sails in hover, but it can recover itself to its initial position and land safely.

After the successful vertical flight tests with good stabilization performance, horizontal flight tests were also carried out. In these tests, SUAVI took off vertically until reaching a reference altitude and then tilted the wings gradually to the angle of attacks of the desired forward speed. During these tests, flights with up to 40 km/h horizontal speed are accomplished and SUAVI is landed safely. Snapshots from a horizontal flight test are presented in Fig. 36. Attitude and altitude references and measurements that are obtained in this test are depicted in Fig. 37a and GPS coordinate reference and measurements are shown in Fig. 37b. It is seen in the figures that the roll reference was changed for the tracking of GPS reference, whereas the pitch reference is kept at 0° during the horizontal flight. It is also observed that the errors in roll, pitch and heading reference tracking were bounded by 6°, which is quite reasonable in the existence of gusts, and that altitude reference tracking was quite satisfactory. Note that the measured position tracking is curved (Fig. 37b) due to the cross wind during the flight.

It should be noted that a filter (typically the EKF) is needed to smooth out the GPS position and velocity estimate for a stable take-off and landing. To this end, GPS measurements can be combined with the IMU or camera measurements in the EKF algorithm to generate smooth GPS position and velocity estimates. It should also be noted that there is a camera in our system that performs vision based control tasks such as takeoff and landing. At the moment, stable takeoff and landing are achieved using sonar and vision measurements.

6. Conclusion and future work

The work reported in this paper presents aerodynamic and mechanical design, prototyping and flight control system design of a new unmanned aerial vehicle (SUAVI) that can vertically take-off and land like a quad-rotor helicopter and horizontally fly like an airplane. The aerodynamic design of the aerial vehicle is optimized by performing several simulations and wind tunnel tests. The mechanical structure that supports the aerodynamic shape in all flight modes is determined with the wing tilting reliability, lightness and strength against the flight and landing loads under consideration. Prototype of SUAVI is produced using carbon composite material. A full dynamical model of SUAVI is derived by using Newton–Euler formulation for the development of the flight control system. A hierarchical control system that includes high and low-level controllers is developed and implemented in Matlab environment for simulations and in the control hardware of the aerial vehicle for real flight. Performance of the flight control system is verified through various simulations and real flight tests.

As a future work, SUAVI will be tested in various operational scenarios in semi or full autonomous modes.

Acknowledgement

Authors would like to acknowledge the support provided by TUBITAK (Scientific and Technological Research Council of Turkey) under Grant 107M179.

References

[1] Erbil MA, Prior SD, Karamanoglu M, Odedra S, Barlow C, Lewis D. Reconfigurable unmanned aerial vehicles. In: Proceedings of the International Conference on Manufacturing and Engineering Systems; 2009. p. 392–6.
[2] Puri A. A survey of Unmanned Aerial Vehicles (UAV) for traffic surveillance. In: Department of computer science and engineering, University of South Florida; 2008. <http://www.csee.usf.edu/apuri/techreport.pdf>.
[3] ISTAR (Intelligence, Surveillance, Target Acquisition & Reconnaissance). General Dynamics. <http://www.generaldynamics.uk.com/solutions-andcapabilities/istar>.
[4] Salazar S, Lozano R, Escareno J. Stabilization and nonlinear control for a novel Trirotor mini-aircraft. Elsevier Control Engineering Practice. vol. 17; February 2009. p. 886–94.
[5] Latchman H, Wong T. Statement of work for airborne traffic surveillance systems – proof of concept study for florida department of transportation; 2002. <http://www.list.ufl.edu/publications/atss_prop-oct-02-verb.pdf>.
[6] Coifman B, McCord M, Mishalani M, Redmill K. Surface transportation surveillance from unmanned aerial vehicles. In: 83rd Annual meeting of the transportation research board; 2004.
[7] Murphy DW. The Air Mobile Ground Security and Surveillance System (AMGSSS). In: 10th annual ADPA security technology symposium; September 2005.
[8] Travers D. Brigade ISTAR operations. Arm Doctrine Train Bull 3 2000;3(4):43–9.
[9] McGuinness B, Ebbage L. Assessing human factors in command and control: workload and situational awareness metrics. In: Proceedings of the command and control research and technology symposium; 2002.
[10] Crck E, Lygeros J. Sense and avoid system for a MALE UAV" AIAA guidance. In: Navigation and control conference and exhibit; August 2007.
[11] Grigson P, Gray A. CFD analysis of the low-speed aerodynamic characteristics of a UCAV. In: 13th RPVs/UAVs international conference; 1999.
[12] Carroll D, Everett HR, Gilbreath G, Mullens K. editors. Missions, technologies, and design of planetary mobile vehicles; 2006.
[13] Snyder D. The quad tiltrotor: its beginning and evolution. In: Proceedings of the 56th annual forum, american helicopter society. Virginia Beach, Virginia; May 2000.

[14] Lee J, Min B, Kim E. Autopilot design of tilt-rotor UAV using particle swarm optimization method. In: International conference on control, automation and systems, October 17–20. Seoul, Korea; 2007.
[15] Kendoul F, Fantoni I, Lozano R. Modeling and control of a small autonomous aircraft having two tilting rotors. In: Proceedings of the 44th IEEE conference on decision and control, and the european control conference, December 12–15. Seville, Spain; 2005.
[16] Dickeson JJ, Miles D, Cifdaloz O, Wells VL, Robriguez, AA. Robust LPV H gain-schedules hover-to-cruise conversion for a tilt-wing rotorcraft in the presence of CG variations. In: Proceedings of the American control conference; July 2007.
[17] Muraoka K, Okada N, Kubo D. Quad Tilt Wing VTOL UAV: aerodynamic characteristics and prototype flight test. In: AIAA unmanned...unlimited conference, April 9. Seattle, Washington; 2009.
[18] Suzuki S, Zhijia R, Horita Y, Nonami K, Kimura G, Bando T, et al. Attitude control of quad rotors QTW–UAV with tilt wing mechanism. J Syst Des Dynam 2010;4(3):416–28.
[19] McCormick BW, editor. Aerodynamics, aeronautics, and flight mechanics. New York (NY): Wiley; 1995.
[20] Anderson JD, editor. Fundamentals of aerodynamics. Boston (MA): McGraw-Hill; 2001.
[21] Franklin JA, editor. Dynamics, control, and flying qualities of V/STOL aircraft. Reston (VA): American Institute of Aeronautics and Astronautics; 2002.
[22] Madani T, Benallegue A. Backstepping control for a quadrotor helicopter. In: IEEE/RSJ international conference on intelligent robots and systems; 2006. p. 3255–60.
[23] Bresciani T. Modeling identification and control of a quadrotor helicopter. Master Thesis, Department of automatic control. Lund University; 2008.
[24] Bouabdallah S, Siegwart R. Full control of a quadrotor. In: IEEE/RSJ international conference on intelligent robots and systems; 2007. p. 153–8.
[25] Kendoul F, Fantoni I, Lozano R. Asymptotic stability of hierarchical inner-outer loop-based flight controllers. In: Proceedings of the 17th IFAC world congress; 2008. p. 1741–46.
[26] Kalman RE. A new approach to linear filtering and prediction problems. J Basic Eng 1960;82:35–45.
[27] Simon D. Optimal state estimation, Kalman, H_∞ and nonlinear approaches. Hoboken (NJ): John Wiley & Sons Inc.; 2006.
[28] Steven L. Waslander, Carlos Wang. Wind disturbance estimation and rejection for quadrotor position control. In: AIAA Infotech@Aerospace conference and AIAA unmanned...unlimited conference. Seattle, WA; April 2009.

Please cite this article in press as: Cetinsoy E et al. Design and construction of a novel quad tilt-wing UAV. Mechatronics (2012), http://dx.doi.org/10.1016/j.mechatronics.2012.03.003